# WHEN WRONG ANSWERS REMAIN UNSETTLED: FAILURE DYNAMICS IN RECURRENT REASONERS

**Anonymous authors**
Paper under double-blind review

## ABSTRACT

Weight-shared recurrent models allocate additional computation by iterating the same blocks, but a wrong terminal answer need not be a settled one. We measure answer persistence under continued recurrence in a trained Hierarchical Reasoning Model (HRM; 27M parameters, Sudoku-Extreme), comparing perturbed continuation with an unperturbed control. After one additional inference budget, mild wrong answers persist at a rate of $0.42$ ($n = 170$), versus $0.95$ for solved endpoints ($n = 512$); the rate pooled over $512$ wrong endpoints is $0.18$. Perturbations spanning $0.05$–$20\times$ the terminal-update scale have little effect on these rates. The measurement therefore primarily reflects finite-horizon answer persistence, rather than sensitivity to perturbation or asymptotic attraction. Solved HRM endpoints have a mean leading-Ritz radius of $0.44$, while scheduled linear models predict fast-loop updates better than slow-loop updates (held-out $R^2 = 0.72$ versus $0.37$). We also evaluate established perturb-and-reselect procedures with paired gains, regressions and oracle headroom. The frozen noise recipe gains $4.8$ accuracy points ($197$ gained, $2$ lost); compute-matched extended depth gains $5.6$, and Sudoku symmetry augmentation gains $34.6$. Across six evaluated settings, solved answers remain more persistent than wrong answers, but the fixed persistence threshold and HRM spectral and timescale patterns do not generalise universally. TRM and GRAM-guided TRM share a module across their two levels. The timescale ordering reverses on unsolved TRM states and in the GRAM-guided setting; in TRM both injection sites give similar gains. These results separate terminal-answer persistence, local geometry and reselection efficacy, and delimit which failure diagnostics transfer across recurrent models.

## 1 INTRODUCTION

Recurrent-depth models increase inference computation by iterating weight-shared blocks, from Universal Transformers (Dehghani et al., 2019) to HRM (Wang et al., 2025) and latent recurrent-depth models (Geiping et al., 2025; Saunshi et al., 2025). Unlike a standard transformer's sequence of distinct operators (nostalgebraist, 2020; Belrose et al., 2023), a tied map $z_{t+1} = f(z_t, x)$ defines a dynamical system that can be analysed directly (Sussillo & Barak, 2013). This provides a way to study how test-time compute (Snell et al., 2024) changes a prediction, including whether further iteration approaches a fixed point (Bai et al., 2019).

When such a model returns a wrong answer, has its computation settled? Recent studies describe failure in terms of attractor entrapment, bounded non-convergence, or continued exploration (Efstathiou & Balwani, 2026; Sghaier et al., 2026; Corbett et al., 2026). These descriptions concern different properties of the trajectory and need not be mutually exclusive. In particular, a flat decoded-loss curve or a clustered PCA projection does not establish that the terminal answer persists under further recurrence (Sec. 2).

We measure this persistence directly, comparing perturbed continuation with an unperturbed control (Sec. 4). In the primary HRM checkpoint, wrong terminal answers are substantially less persistent than correct ones. Endpoint Jacobian–vector products characterise the local linearisation (Sec. 5); progressively richer linear models isolate which transient updates remain poorly predicted (Sec. 6). We relate these updates to constraint propagation (Sec. 7) and evaluate perturbation and reselection against compute-matched alternatives (Sec. 8).



Reviewers: please read the Reviewer Guidelines (iclr.cc/Conferences/2027/ReviewerGuidelines) and the AI Policy for Reviewers (iclr.cc/Conferences/2027/AIPolicyForReviewers). If you used AI to expand, edit, or polish your review, please provide the input text to the LLM. Better still, consider skipping the LLM and submitting your original text: we, and the authors, are much more interested in your unedited thoughts than in what an LLM has to say. AI-assisted or not, you are putting your name and reputation behind your review: LLM-generated falsehoods, hallucinations or misrepresentations are subject to disciplinary action, which may include desk-rejecting all papers you have authored.

**Contributions.**

1. **Answer persistence with an unperturbed control.** After one additional inference budget, mild wrong answers persist at $0.42$ versus $0.95$ for solved endpoints ($n$=170 and $512$; $0.18$ pooled over all $512$ wrong endpoints). Perturbations up to $20\times$ the update scale have little effect on these rates. The measurement therefore primarily reflects continuation. The solved–wrong ordering holds across six evaluated settings, although a majority-persistence threshold does not (Fig. 2; Apps. M, P).
2. **Local and transient dynamics, with transfer limits.** Solved HRM endpoints have a mean leading-Ritz radius of $0.44$. Scheduled linear models predict fast-loop updates better than slow-loop updates (held-out $R^2$=0.72 versus $0.37$). These geometric patterns change in TRM and GRAM-guided TRM, limiting their use as general explanations of failure (Secs. 5–6).

Perturb-and-reselect procedures are established prior work (Efstathiou & Balwani, 2026; Sghaier et al., 2026; Corbett et al., 2026). Our evaluation adds paired gains and regressions, injection-site comparisons, oracle headroom, and compute-matched baselines: noise injection gains $4.8$ points (197 gained / 2 lost), while extended depth performs better. We also document mean-field pooling and incomplete clock conditioning as sources of misleading dynamical summaries, with synthetic regression tests (App. A).

## 2 Related Work

**Recurrent-depth models and their dynamics.** HRM (Wang et al., 2025) and TRM (Jolicoeur-Martineau, 2025) reuse parameters across recurrent updates, building on universal transformers (Dehghani et al., 2019) and adaptive computation time (Graves, 2016), with related equilibrium formulations in deep equilibrium models (Bai et al., 2019). Recent work scales latent depth (Geiping et al., 2025) and asks how looped models use it (Blayney et al., 2026; Csordás et al., 2025; Pappone et al., 2025; Kapl et al., 2026; Knupp et al., 2026). Ren & Liu (2026) study HRM's trajectory geometry and input sensitivity; we examine endpoint spectra and whether a terminal state keeps its answer when continued or perturbed. The input-perturbation effect they report independently is what our input-site injection probes, separately from injection into the recurrent state (App. K). Fixed-point linearisation (Sussillo & Barak, 2013) has limited reach away from equilibrium (Caruso & Jarne, 2023), motivating trajectory-level analyses (Ostrow et al., 2023; Maheswaranathan et al., 2019). Whereas Jacobian-switching LDS (Smith et al., 2021) uses state-dependent linearisation, our full-clock test fits operators indexed by the update schedule, capturing HRM's fast $z_L$ updates better than its slow $z_H$ updates (Sec. 6).

**Perturbation and reselection.** Sample-and-select methods (Wang et al., 2023) require diverse candidates. For deterministic HRM, these can come from task symmetries (App. J) or noise; GRAM (Baek et al., 2026) incorporates stochasticity into the recurrence. Prior methods perturb the answer initialisation and scale the number of attempts (Efstathiou & Balwani, 2026), inject noise throughout recursion (Sghaier et al., 2026), or use online particle filtering (Corbett et al., 2026), with learned halting scores guiding selection. Our independent reruns use a single injection and terminal halting-head selection. We add paired gains and regressions, site comparisons and compute-matched alternatives, alongside an exploratory timing analysis (App. K). Candidate diversity and guide quality are also studied in prior work; we do not claim to introduce that distinction.

**Descriptions of failure and terminal-answer persistence.** Prior work discusses attractor entrapment (Efstathiou & Balwani, 2026), bounded non-convergence (Sghaier et al., 2026), and continued exploration (Corbett et al., 2026). Efstathiou & Balwani (2026) state that on Sudoku-Extreme "failed runs plateau at stable high-loss attractors rather than continuing exploration", which is the description our measurement addresses. We quote their abstract; their full text was unavailable, so we do not describe the experiments behind it (App. U). Corbett et al. (2026) provide tube-stability diagnostics under a contraction assumption. Our endpoint spectra address a different quantity: a local leading-eigenvalue estimate, rather than a uniform contraction bound along a trajectory. The two cannot be substituted for one another. We test whether the terminal decoded answer persists beyond the

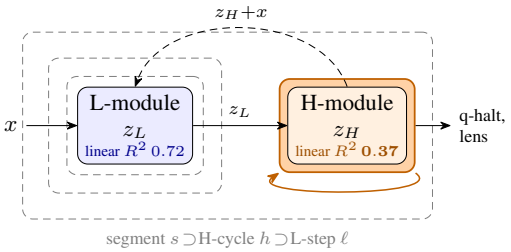


*three injection sites; over* 41.6%:
inject $x$ −1.1 pts, **243** lost
inject $z_L$ +2.9 pts, 1 lost
inject $z_H$ +4.6 pts, 2 lost
*no injection, same* 9× *budget:*
depth alone +5.6 pts, 14 lost
depth, best seg. +**6.0** pts, 2 lost ← beats all three

(a) mechanism → site → gain

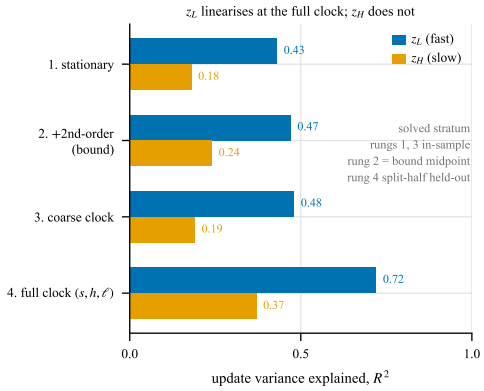


(b) progressive exclusion of linear descriptions

Figure 1: **Overview. (a)** HRM iterates two weight-tied modules on an exogenous three-level clock, the input injection $z_H+x$ entering the fast L-module each step; shaded is the slow $z_H$ loop, which (b) isolates. Site gains: one $k=8$ run at matched radii, $N=4096$ (App. K). Recurrent states are perturbed after five segments; input is perturbed before recurrence and remains perturbed throughout. Depth is evaluated in App. L; Sec. 8's headline $+4.8$ is this same $z_H$ site under the frozen recipe. The site axis identifies *why* the input site fails, not the best use of a test-time budget. **(b)** Excluding successively stronger linear descriptions of the update trajectory leaves the slow loop least captured: held-out $R^2=0.37$ for $z_H$ against 0.72 for the fast $z_L$, a close-to-scheduled linear program.

trained budget, using an unperturbed control to distinguish continuation from noise effects. Finite continuation does not establish the absence of asymptotic attractors (App. N).

## 3 Background and Experimental Setup

**Model and task.** The Hierarchical Reasoning Model (HRM) is a 27.3M-parameter recurrent transformer of two coupled recurrences (a fast L-module and a slow H-module) wrapped in an adaptive-computation-time (ACT) outer loop with a learned q-halt head. Blocks are post-norm with RMSNorm; the recurrences couple by additive input injection, $z_H+x$ into the L-module each L-step and $z_L$ into the H-module once per H-cycle. We study the released configuration $H=2$, $L=2$ with up to 16 ACT segments, trained on Sudoku-Extreme (1000 puzzles × 1000 augmentations; vocab 11, sequence length 81) for 20,000 epochs on a single RTX 6000 Ada (10h44m; global batch 384, lr 7e−5; no pretraining, no chain-of-thought). An epoch is one pass over the 1000 base puzzles, not over the augmented million: 52,080 steps at batch 384 is 1000 examples per epoch. We analyse checkpoint `step_52080` (epoch 20,000), which attains exact accuracy 41.76% (per-cell 79.92%, q-halt accuracy 99.46%) on the full 422,786-puzzle test set. The primary run uses seed 0, `lr_min_ratio=1.0` and `weight_decay=1.0`; the remaining configuration is recorded with the checkpoint.

**What was run.** Body measurements are HRM/Sudoku-Extreme, seed-0. The same diagnostics run unchanged on five further settings—a second seed, a second architecture (TRM), a second task (Maze-30×30-Hard), a GRAM-guided recurrence, and a third task (N-Queens-10×10). Fig. 2 is which of the five claims each one carries. A sixth, N-Queens-12×12, did not train and is reported as a null (App. Q). The intervention is reported against compute-matched alternatives—depth alone (App. L) and symmetry augmentation (App. J)—and the stationarity rates against two controls: an unperturbed rerun (App. M) and continuation to 128× the trained budget (App. N). Thirteen of the 63 job scripts behind these carry an interpretation rule committed before execution (App. I).

**Three timescales and notation.** An exogenous clock nests the computation into three levels (ACT segment $s\in\{1..16\}$, H-cycle $h$, L-step $\ell$, with $H=L=2$; Fig. 1(a)), driving two coupled updates,

$$z_L \leftarrow \mathrm{L}(z_L,\, z_H+x), \qquad z_H \leftarrow \mathrm{H}(z_H,\, z_L). \tag{1}$$




Figure 2: **What travels.** Each claim against the settings that can carry it—disc holds, cross fails, query undecided—tallied over the settings that returned a verdict. The two that break the geometry are the two that share a collapsed module. Values, $n$ and caveats: Fig. 15.

We study the residual-stream updates $\Delta z_t{=}z_{t+1}{-}z_t$ at each level's timescale ($z_L$ within an H-cycle, $z_H$ across H-cycles, $z_{\text{ACT}}$ across segments). Hidden states are 512-dimensional at each of 81 Sudoku cells (plus a puzzle embedding); every statistic treats each $(t, \text{position})$ update as one sample.

**Reduction discipline (read first).** All trajectory statistics use *per-position* resolution; position-averaged ("mean-field") reductions inflate linearity and complex mass and are shown only where flagged (see App. A).

**Evaluation samples.** Unless noted, analyses draw on a stratified sample of 512 solved and 512 unsolved puzzles, the unsolved bucketed by wrong-cell count (1–5 / 6–20 / >20); the recomputed solved rate matches the official 41.76% to within 0.1pt. Intervention deltas use a disjoint uniform 4,096-puzzle subset. Every $\Delta$ in points is paired on those same puzzles: $\Delta{=}100(b{-}c)/N$ for $b$ gained (wrong→right) and $c$ lost, on *exact* (whole-grid) accuracy; intervals use a paired normal approximation, $\text{Var}(\Delta){=}10^4(b{+}c{-}(b{-}c)^2/N)/N^2$, while regression *rates* use Wilson.

**Two senses of "settled".** The *terminal-update gate* asks whether the last step is small: $\|\Delta z_{\text{final}}\|/\|z\| \le q_{95}$, for $q_{95}$ the 95th percentile of that *relative* ratio over solved endpoints. Post-norm RMSNorm pins $\|z\|$, so the denominator varies little and the cut is close to an absolute one on $\|\Delta z_{\text{final}}\|$ (App. E). *Stationary* asks whether continued computation leaves the state where it is (Eq. 3). They are not the same question: 95% of solved but also 69% of wrong endpoints clear the gate (App. G), and Sec. 4 is about that gap. We call these *gate-passing* states; the data-calibrated gate does not certify a fixed point.

## 4 Terminal-Answer Persistence and Correctness Prediction

**Wrong terminal answers are less persistent than correct ones.** We compare decoded-answer persistence, $R_{\text{ans}}$, with state persistence, $R_{\text{state}}$. The latter uses a setting-specific distance scale and is not directly comparable across models (Sec. 9). Reselection is evaluated separately in Sec. 8.

**One stationarity test.** Let $z_i^*$ be the terminal $z_H$ of endpoint $i$, $\Phi$ the recurrence of Eq. 1 run for a further 16 segments (the trained budget, fixed for every endpoint rather than re-halted by ACT), $\hat{y}(\cdot)$ the decoded answer on the answer mask, $S$ the number of state entries (82 positions $\times$ 512 channels $=$ 41,984), and $\kappa$ one *global* scale, the median $\|\Delta z_{\text{final}}\|$ over the analysed endpoints. The kick enters $z_H$ alone and $z_L$ passes into the continuation unchanged, so $\varepsilon{=}0$ reproduces the continuation the model itself would run. *Perturb and continue:*

$$z_{i,\varepsilon} = \Phi\big(z_i^* + \varepsilon\kappa S^{-1/2}\xi\big), \quad \xi \sim \mathcal{N}(0, I_S), \quad \mathbb{E}\big\|\varepsilon\kappa S^{-1/2}\xi\big\|^2 = \varepsilon^2\kappa^2. \tag{2}$$

The factor $S^{-1/2}$ makes the root-mean-square perturbation norm $\varepsilon\kappa$, independently of state dimension.

*Score the answer, then the class:*

$$r_i(\varepsilon) = \Pr_\xi\big[\hat{y}(z_{i,\varepsilon}){=}\hat{y}(z_i^*)\big], \qquad R_{\text{ans}}^{(C)}(\varepsilon) = \tfrac{1}{|C|}\textstyle\sum_{i\in C} r_i(\varepsilon). \tag{3}$$

**Every rate we report is the class-level $R^{(C)}$**; $R_{\text{state}}$ is the same with $\|z_{i,\varepsilon}-z_i^*\|<\kappa$ replacing the answer test. *Now set $\varepsilon$=0:*

$$R_{\text{ans}}^{(C)}(0) = \tfrac{1}{|C|}\big|\{\, i \in C :\ \hat{y}(\Phi(z_i^*))=\hat{y}(z_i^*)\,\}\big|. \tag{4}$$

For the deterministic recurrence, $r_i(0)$ is binary and the class rate is the fraction retaining its answer after one additional budget. We use $R_{\text{ans}}^{(C)} > \frac{1}{2}$ as a descriptive *majority-persistence* criterion. It is a population summary, not an attractor definition. Equality at the two readouts also does not exclude intermediate answer changes.

The terminal-update gate and answer persistence address different questions: $69\%$ of wrong HRM endpoints pass the former, yet most fail the latter. Neither test alone certifies asymptotic stability.

**Failure taxonomy.** Gate failure rises with error severity but stays a *minority* in every bucket—$21\%$ of mild failures, $29\%$ at 6–20, $43\%$ beyond (App. G)—so the dominant failure mode is *small-step-but-wrong*.

**Persistence and replication.** Solved endpoints retain their decoded answer at $R_{\text{ans}} = 0.95\,[0.93, 0.97]$ and remain within the state-distance threshold at $R_{\text{state}} = 0.86\,[0.82, 0.88]$. For mild wrong endpoints these rates are $0.42\,[0.35, 0.49]$ and $0.13$ (endpoint-clustered bootstraps; $n = 512$ solved and 170 mild wrong). Mild is the most persistent wrong bucket under both dump and replay labels. The other dump-labelled buckets score $0.09$ and $0.04$, but their ordering reverses under replay labels (App. H). The pooled rate of $0.18$ refers to the stratified sample.

Across 13 radii in $[0.05, 20]$ and 12 seeds, persistence changes little; the median solved-state displacement changes by $0.8\%$ between $\varepsilon = 0$ and 20 in the pilot (App. M). In longer continuation, wrong answers persist across equal 128-segment windows at a mean rate of $0.43$, versus $0.97$ for solved endpoints, through $2048$ segments (App. N). This measures agreement between readouts, not progress toward correctness.

The solved–wrong ordering also appears in TRM ($0.96/0.32$ answer persistence; $0.32/0.02$ state persistence) and Maze. Absolute state rates vary substantially across settings. The answer-level $\frac{1}{2}$ criterion separates the four Sudoku- and Maze-based settings at every tested radius, but fails on N-Queens-$10 \times 10$ ($0.96/0.56$) and GRAM-guided TRM ($0.98/0.84$). Thus the observed ordering transfers across six settings; the fixed cut does not (Fig. 15). Both also reproduce the control: unperturbed continuation returns $0.59$ for N-Queens' wrong class against $0.56$ perturbed, and $0.84$ for the GRAM-guided recurrence against $0.83$ at the control's own matched radius, so what the rates measure there is persistence and not perturbation sensitivity, as on HRM. Severity mixtures still differ between settings, so the replications remain a qualitative ordering.

**Does the model know? Probes vs. q-halt.** A linear probe trained on the final $z_H$ (group 5-fold CV) reads correctness at AUROC $0.941$ overall and $0.887$ on the mild small-step-but-wrong failures, barely above the model's own halting head ($0.934$ and $0.873$ on the same splits; that margin shrinks to zero under replay labels, App. H). The tested linear probe therefore adds little to q-halt on these samples. This does not establish optimality over all linear readouts or absence of correctness information: trajectory features and nonlinear readouts improve discrimination (App. O).

## 5 Local linearisation at terminal states

**Method.** We linearise the per-iteration H- and L-updates about solved endpoints $z^*$ and wrong terminal states, which need not be exact roots. Rather than materialise the $(SD) \times (SD)$ Jacobian $\partial f/\partial z$ we probe it with Jacobian–vector products and $m$=40 Arnoldi steps, checked against a dense eigendecomposition, and summarise each spectrum by $\hat{\rho}_{40} = \max_i |\theta_i|$ over the retained Ritz values and their complex fraction (256 endpoints per class, both maps $f_H, f_L$). Even at solved endpoints, $\hat{\rho}_{40} < 1$ does not rule out expanding modes missed by the Krylov subspace and is not a stability certificate. The terminal-update gate provides residual information, not a bound on unobserved modes.

**Results** (App. Fig. 10; per-example complex-plane spectra in App. G): solved $f_H$ has low estimated radii (mean $\rho$=0.44, every gate-passing endpoint below $0.90$, $65\%$ of retained Ritz values complex;

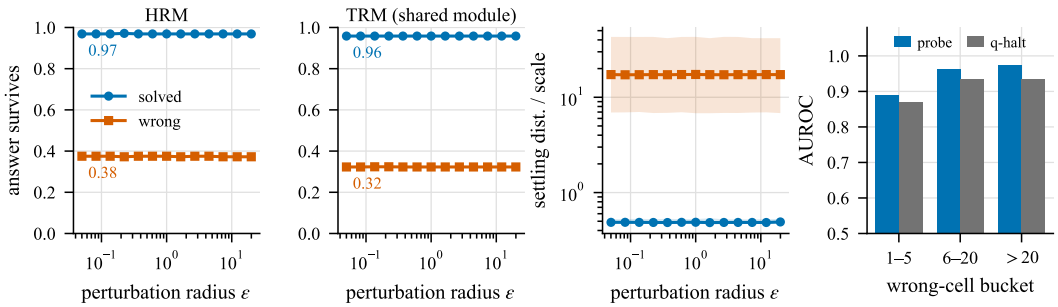


Figure 3: Failure structure (solved vs. wrong). **(a, b) The central criterion:** $R_{\text{ans}}$, the fraction of continuations whose decoded answer survives, against the radius $\varepsilon$ of an optional perturbation (13 radii $\times$ 12 seeds $\times$ 32 endpoints/class; 96 for TRM). *The lines are flat because $\varepsilon$ does not matter*: the axis starts at $\varepsilon$=0.05, and the separately-run unperturbed control returns these same rates (0.97/0.38; App. M), so what is measured is whether the terminal decoded answer settles under continued recurrence. TRM preserves the *ordering*, not the magnitude. The interval-bearing rates in the text come from the 512-endpoint replication (App. M), which trades radii for $n$. **(c)** State-level graded form (median, IQR). **(d)** A correctness probe on $z_H$ barely beats the model's own halting head.

$f_L$ mean $\rho$=0.78), while wrong $f_H$ has mean $\hat{\rho}_{40}$=0.75 (median 0.77) with 2.7% showing an estimated expanding leading mode ($\hat{\rho}_{40}>1$; 7/256, 95% CI [1.3, 5.5]%) and 9.4% above 0.9. The tail is *not* exclusive to failures: raw it points both ways, and gated it is one-sided, 0/243 solved vs. 4/176 wrong (App. G). The summary we rely on is neither tail but the distributional one: AUC=0.913, 95% bootstrap CI [0.886, 0.940], unchanged under replay labels (0.928; App. H).

At solved endpoints with small final updates, these estimates are consistent with locally damped dynamics containing oscillatory modes. They do not certify an exact fixed point, Euclidean contraction, or stability of the coupled recurrence. We next examine the transient preceding these endpoints (App. Fig. 6).

## 6 Transient Dynamics Across Linear Model Families

We compare progressively richer linear descriptions of per-position updates along the transient and identify the streams they predict least well. Sec. 8 evaluates interventions at those sites.

### 6.1 Excluding Time-Invariant, Second-Order, and Coarse-Clock Linear Descriptions

A single time-invariant operator $\Delta z_{t+1} \approx A\Delta z_t$ (streaming least-squares $A=C_1C_0^+$, uncentred one-step $R^2$) fits poorly at per-position resolution, explaining only $R^2$=0.43/0.18/0.12 of the update variance for $z_L/z_H/z_{\text{ACT}}$; position-averaging inflates these to 0.90/0.49/0.38, a pooling artifact (App. A). The residual is as high-rank as the signal, so no low-dimensional dropped modes recover it, and a second-order term ($\Delta z_{t+1}$ from $[\Delta z_t, \Delta z_{t-1}]$) captures only 5–10% of it: linear memory does not account for it either. These tested linear families leave substantial residual variation.

The recurrence has an explicit clock, so the operator could be piecewise-linear, switching by phase; but conditioning on a *coarse* phase recovers almost nothing and yields operators stable across puzzles yet drifting across trajectory time, superficially the fingerprint of state-dependent nonlinearity. This is a trap: trajectory time *is* the pooled-away clock, so a fully scheduled but purely *linear* $A(s, h, \ell)$ reproduces the signature with no state dependence (App. A).

### 6.2 The Full-Clock Test Leaves the Slow Loop Substantially Less Linearisable

We close the loophole by bucketing every update by its complete clock $(s, h, \ell)$ (segment, H-cycle, L-step), yielding 62 $z_L$ and 30 $z_H$ per-position operators (64/32 snapshots give 63/31 updates, and pairing consecutive updates leaves 62/30 buckets, a structural count that precedes any energy or

reliability filter; App. C), each fit on ≥41,984 vectors (≈81:1). Because the noise-dominated near-fixed-point tail swamps an unweighted median, we summarise by the energy-weighted mean over the top-tercile ticks $\mathcal{T}$ (per-tick energy $E_\varphi = \sum_{t\in\varphi} \|\Delta z_t\|^2$),

$$R^2_{\text{hi}} = \frac{\sum_{\varphi\in\mathcal{T}} E_\varphi \, R^2_\varphi}{\sum_{\varphi\in\mathcal{T}} E_\varphi}, \tag{5}$$

and de-bias for conditioning by a split-half check: each puzzle-half's operator scored on the other half,

$$R^2_{\text{ho}} = \tfrac{1}{2}\big[R^2(A_{\text{e}}; \text{o}) + R^2(A_{\text{o}}; \text{e})\big], \quad R^2_{\text{corr}} = R^2_{\text{ho}} / R^2_{\text{in}}. \tag{6}$$

**Result** (Fig. 4). The fast recurrence's linearity concentrates where the energy is: its top-3 ticks carry $51\%$ of all update energy. The concentration is not a monotone trend (Pearson $+0.76$, rank $-0.29$), which we report because the same rank test demotes a claim below. Split-half correction leaves the gap intact (held-out $+0.35$ vs. raw $+0.33$; App. Fig. 7), so in-sample optimism does not produce it. Held-out $R^2$ still tracks each bucket's signal-to-noise ratio and does not separate unpredictable variation from nonlinearity. The one apparent asymmetry (for $z_H$, energy–linearity alignment $+0.03$ solved vs. $+0.88$ unsolved) is a fixed-point-tail effect plus a leverage artifact (App. C). The robust difference is dynamical: unsolved sustains high-energy poorly-captured updates late (segment $>8$: median energy $\approx 4.5\times$ solved's, $R^2 \approx 0.21$), consistent with continued search, while solved's updates have decayed.

**Conditioning on the input drive.** Adding the injection $z_H + x$ to the per-tick regression does not improve held-out prediction at the two highest-energy $z_L$ ticks ($\Delta R^2 = -0.003$; App. D). This supports the predictive contribution of the previous update, but redundant predictors do not establish causal independence from the drive.

**Scope of the timescale comparison.** The tested predictors leave more residual variation in HRM's slow $z_H$ updates than in its fast $z_L$ updates. Kernel and MLP refits recover approximately $0.03$ additional held-out $R^2$ (App. D). This motivates the site comparison in Sec. 8, but does not identify a causal role for the residual. Across-puzzle operator drift is dominated by conditioning and is not used as a state-dependence diagnostic (App. B).

The default slow-loop estimates use only 1–3 reliable high-energy ticks. Relaxing the energy and reliability thresholds retains 10–14 ticks while preserving the HRM ordering (App. F). Composing fast updates onto the slow clock removes $37\%$ of the solved gap, leaving $0.22$ (App. E). The ordering recurs across HRM seeds and attenuates on the published Maze checkpoint, though not on two others (App. S), and reverses on unsolved TRM states. It is a property of the measured settings and estimator, not a universal division of computation.

## 7 Relation to constraint propagation

The later iterations carry the harder part of the computation. Running a naked/hidden-singles propagator to fixation on each solved puzzle, the segment at which the model's lens commits a cell—the first segment whose H-lens argmax for that cell is correct and stays correct to the last—tracks its propagation depth (within-puzzle Spearman $\rho = 0.32$). The model does more than propagate: only $20.9\%$ of solved puzzles are fully singles-determined, and the cells the propagator leaves unforced resolve substantially later than the forced ones (6.3 vs. 2.1). Search-like work thus concentrates in the later iterations, where the fits are weakest (Sec. 6; counts and tests in App. Figs. 8, 9).

## 8 Reselection and compute-matched alternatives

Perturbation and reselection can generate and select alternative predictions (Efstathiou & Balwani, 2026; Sghaier et al., 2026; Corbett et al., 2026). This experiment differs from the persistence test: it injects after five of 16 segments (zero-based index 4) and scores correctness, whereas Sec. 4 continues terminal states and scores agreement with their original answers. High terminal persistence does not preclude reselection gains, as GRAM-guided TRM demonstrates (App. T).

**Four procedures, one selector** (Fig. 5; uniform $N = 4096$, all oracle-free, reselected by the model's own halting logit). Injecting noise into $z_H$ mid-run gives $+4.8$ points (197 gained, 2 lost). The

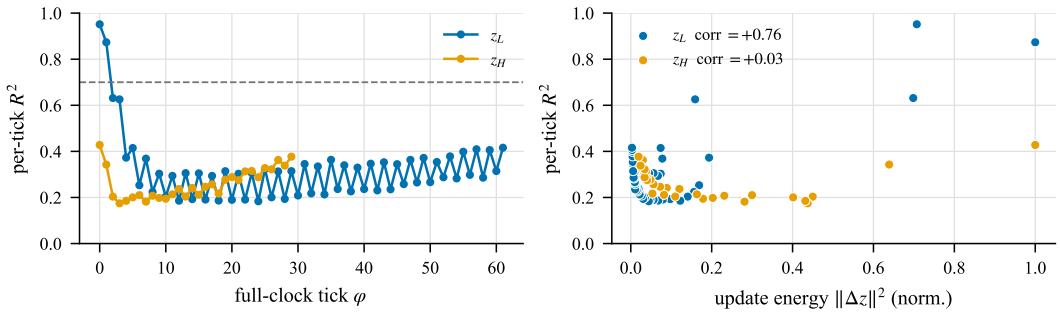


Figure 4: Full-clock per-tick linear fits, solved stratum, *raw* per-tick $R^2$. **Left:** $R^2$ along the clock $\varphi$ (62 $z_L$ ticks against 30 $z_H$). **Right:** the same $R^2$ against that tick's update energy $\|\Delta z\|^2$. The fast $z_L$ recurrence's linearity *rises* with energy (Pearson $+0.76$, peak $0.95$), so the energy-weighted summary is carried by the ticks that do the work; the slow $z_H$ shows no such structure ($+0.03$) and stays weakly fit even where it is most energetic. The split-half-corrected energy-weighted figures ($0.72$ against $0.37$) and the estimator behind them are in App. C.

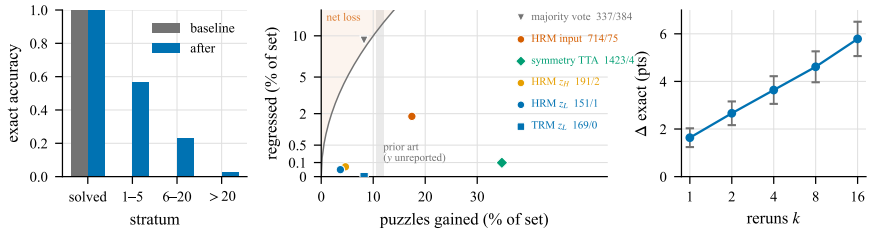


Figure 5: Oracle-free noise reselection, $k$=8, reselected by the model's own halting logit. **Left:** exact accuracy by stratum, balanced 1024-puzzle sample; the gain decays with severity ($+56$, $+23$, $+3$ points). Uniform $N$=4096: $+4.76$, paired 95% CI $[+4.10, +5.42]$. **Middle: the accounting, which is what we claim.** Gained vs. *regressed* puzzles (fraction of set, $\sqrt{\cdot}$ on $y$; solid = break-even); sites are at unmatched $\varepsilon$, and App. K matches their radii. Prior work reports no regression count, so the band gives only the constraint implied by its net gain. **Right:** monotone in budget ($+1.6 \to +5.8$, $k$=1 $\to$ 16); the $k$=8 point ($+4.6$) is an independent draw of the same puzzles.

*same* $9\times$ budget spent on depth alone—running the recurrence to 144 segments with no perturbation anywhere, $9\times$ the trained horizon and so an extrapolation (App. L)—gives $+5.6$ (245/14), and reading out the max-q-halt segment of that single pass gives $+6.0$ (248/2; App. L). These procedures match total recurrent computation but differ in available parallelism and potential latency; App. L specifies the extended-horizon implementation and its extrapolation limits. A task-specific symmetry augmentation gives $+34.6$ (1423/4) and largely *subsumes* the injection: pooling all 17 candidates adds only $+0.51$ over symmetry alone, with selected accuracy consistent with the candidate oracle ceiling (nine-orientation oracle union 76.5%; App. J). We therefore do not claim noise injection as the best use of a test-time budget. Depth corrects 245 baseline errors and introduces 14 regressions, demonstrating that some terminal errors remain recoverable by continuation. Compute matching does not imply latency matching: the 144-segment trajectory is sequential, whereas the $k$=8 perturbed continuations can run in parallel after a shared prefix, subject to hardware and memory constraints. Parallel execution trades additional resources for potentially lower latency; we do not measure hardware-specific wall-clock performance.

**Candidate generation versus ranking.** At $z_H$, q-halt recovers 99.0% of the improvement available in the oracle union (the set of puzzles solved by at least one candidate). Under site-relative scaling, input injection creates a larger oracle union (0.484 versus 0.462), but selection yields a net loss and recovers $-16\%$ of its headroom (App. K). The input-site failure is therefore a ranking limitation; distribution shift in the scored states is a possible explanation. Within-puzzle q-halt spread differs between recoverable and unrecoverable errors (App. U), but does not alone explain selection. Per-cell majority voting over noisy reruns loses 0.51 points.

**Where to inject, and where that stops.** Two lost against one out of $4096$ carries no statistical content, so we scored both recurrent sites on the *full* $422{,}530$-puzzle frame. The rates separate, and not in the direction the timescale split would suggest: $z_H$ regresses $0.0090\%$ (Wilson $[0.0066, 0.0123]$) against $z_L$'s $0.0036\%$ ($[0.0022, 0.0059]$), $2.5\times$ as often. The timescale split therefore picks the *higher-gain* site ($+4.36$ vs. $+2.91$), not the safer one; among recurrent sites there is a trade (App. K). Both have much lower observed regression rates than the input embedding, net negative at matched magnitude. That localization does not survive module sharing: in TRM, injecting into either loop gives the same lift ($+8.25$ vs. $+8.40$; App. V). Protocol, $k$-sweep, timing and per-site scales: App. K.

## 9 Discussion and Limitations

**Architectural vs. computational hierarchy.** Collapsing HRM's two levels into one shared recurrence costs no accuracy (Jolicoeur-Martineau, 2025), so the *architectural* split is droppable; the *computational* one is what isolates the least-linearisable work, and in HRM the higher-gain injection site with it. Under module sharing that split does not vanish, it *inverts*: the fast $z_L$ loop becomes the less-linearisable stream ($R^2$=0.45 against $0.62$, unsolved stratum; TRM's solved stratum does not invert, $0.48/0.48$), and the intervention still transfers—$+8.25$ $(169/0)$ into $z_L$, an indistinguishable $+8.40$ $(172/0)$ into $z_H$. The method still isolates the loop; only in HRM does that localization also say where to intervene (Apps. V, K).

**Implications and limitations.** Continued depth and diverse reruns can correct some terminal errors, while the halting head recovers much of the available candidate headroom. A nonlinear trajectory readout also improves correctness discrimination (App. O).

The main geometric results concern one $27.3$M-parameter HRM checkpoint. A second seed preserves the reported directions. Maze remains a reduced-scale replication: its unsolved fast–slow gap changes from $0.37$ to $0.04$, and its endpoint spectral gap is inconclusive on $107$ solved mazes. Full-clock refits also find a positive gap without a warm restart; differences between training runs prevent isolating the cause of its changed magnitude (App. S). TRM's spectral ordering disappears under the terminal-update gate, and its timescale inversion is confined to unsolved states. Low held-out $R^2$ establishes limited prediction by the tested families, not a particular computational mechanism or irreducible nonlinearity. The coverage figure now has stored metrics for every cell; the separate third-party GRAM endpoint pilot still requires external materials (App. T).

## 10 Conclusion

Wrong terminal answers in the primary HRM checkpoint are less persistent than correct answers under continued recurrence. An unperturbed control shows that the tested perturbations contribute little to this difference. The solved–wrong ordering extends across the evaluated settings, whereas absolute thresholds, endpoint spectra and timescale geometry do not. Noise, extended depth and task symmetries provide distinct sources of alternative predictions; paired gains, regressions and oracle headroom clarify their benefits and limitations. These results characterise finite-horizon failure dynamics without excluding asymptotic attractors.

## AI Use Statement

LLM assistants were used to implement synthetic generators, analysis code, tests and plotting scripts; develop diagnostic criteria and controls; search and critique related work; and draft and revise the manuscript. Puzzle instances came from released dataset builders, not LLM generation. The paper contains no theorems or proofs.

Primary HRM results were computed by analysis code and checked against its stored outputs. Incomplete artifact coverage for additional analyses is identified in the corresponding appendices. Bibliographic records dated 2025 or later were checked against source records. Detailed descriptions of Sghaier et al. (2026); Corbett et al. (2026); Ren & Liu (2026) were checked against their full texts; Efstathiou & Balwani (2026) is quoted from its published abstract, its full text being unavailable (App. U). These checks do not imply independent human re-derivation of every statement. The

authors directed the research and take responsibility for the complete paper, including any errors. No LLM is an author.

## Ethics Statement

This study analyses small recurrent models on algorithmically generated constraint-satisfaction puzzles. It involves no human subjects, personal data or sensitive data. Its results do not establish transfer to deployed systems.

A halting head that ranks candidates well can still misclassify individual outputs, so its confidence alone is insufficient to establish correctness. Repeated inference also incurs additional compute: our noise-injection procedure uses $9\times$ evaluation compute for a $4.8$-point gain, while the compute-matched Sudoku symmetry baseline gains $34.6$ points. Applications should compare such alternatives before adopting the procedure.

## Reproducibility Statement

The primary checkpoint and training configuration are specified in Sec. 3. Evaluation uses fixed manifests for the stratified $512{+}512$ sample, the disjoint uniform $4096$-puzzle sample, and the $32{+}32$ full-trajectory cross-checks. Recorded activations are stored in `fp32`; the streaming second moments and linear-operator fits accumulate in `fp64`; streaming and direct fits agree to $\max|\Delta R^2| = 1.14 \times 10^{-14}$. The instrumented inference loop is checked against the model forward pass to `bfloat16` tolerance, and the test suite covers the analysis and inference checks. Algorithm 1 specifies the linearity estimator; App. H documents replay labels, inclusion probabilities and weighted bootstraps; App. K gives the frozen intervention protocol; and App. I distinguishes pre-specified analyses from exploratory ones. The model-independent analysis subpackage is tested to import without a deep-learning framework. Stored-artifact gaps for nonlinear readouts, replications and pilots are disclosed in their appendices. Full residual-stream traces are not persisted; reproducing analyses that lack stored metrics requires rerunning the checkpoint.

## References

Junyeob Baek, Mingyu Jo, Minsu Kim, Mengye Ren, Yoshua Bengio, and Sungjin Ahn. Generative recursive reasoning. *arXiv preprint arXiv:2605.19376*, 2026. URL https://arxiv.org/abs/2605.19376.

Shaojie Bai, J. Zico Kolter, and Vladlen Koltun. Deep equilibrium models. In *Advances in Neural Information Processing Systems (NeurIPS)*, 2019. URL https://arxiv.org/abs/1909.01377.

Nora Belrose, Zach Furman, Logan Smith, Danny Halawi, Igor Ostrovsky, Lev McKinney, Stella Biderman, and Jacob Steinhardt. Eliciting latent predictions from transformers with the tuned lens. *arXiv preprint arXiv:2303.08112*, 2023. URL https://arxiv.org/abs/2303.08112.

Hugh Blayney, Álvaro Arroyo, Johan Obando-Ceron, Pablo Samuel Castro, Aaron Courville, Michael M. Bronstein, and Xiaowen Dong. A mechanistic analysis of looped reasoning language models. *arXiv preprint arXiv:2604.11791*, 2026. URL https://arxiv.org/abs/2604.11791.

Mariano Caruso and Cecilia Jarne. Analysing rescaling, discretization, and linearization in RNNs for neural system modelling. *arXiv preprint arXiv:2312.15974*, 2023. URL https://arxiv.org/abs/2312.15974.

Andrew Corbett, Archit Sood, Anna Tzatzopoulou, Sai-Aakash Ramesh, and Tim Dodwell. Boosting inference with guided reasoning: Stochastic exploration for recursive models. In *ICML 2026 Workshop on Structured Probabilistic Inference and Generative Modeling (SPIGM)*, 2026. URL https://arxiv.org/abs/2605.25230.

Róbert Csordás, Christopher D. Manning, and Christopher Potts. Do language models use their depth efficiently? In *Advances in Neural Information Processing Systems (NeurIPS)*, 2025. URL https://arxiv.org/abs/2505.13898.

Mostafa Dehghani, Stephan Gouws, Oriol Vinyals, Jakob Uszkoreit, and Łukasz Kaiser. Universal transformers. In *International Conference on Learning Representations (ICLR)*, 2019. URL https://arxiv.org/abs/1807.03819.

Andreas Efstathiou and Aishwarya Balwani. Recursive reasoning as attractor landscape search: Mechanistic dynamics of the tiny recursive model. In *ICLR 2026 Workshop on Latent & Implicit Thinking (LIT)*, 2026. URL https://openreview.net/forum?id=kKps9W1K7n. Quoted from the published abstract; full text not retrieved.

Jonas Geiping, Sean McLeish, Neel Jain, John Kirchenbauer, Siddharth Singh, Brian Bartoldson, Bhavya Kailkhura, Abhinav Bhatele, and Tom Goldstein. Scaling up test-time compute with latent reasoning: A recurrent depth approach. In *Advances in Neural Information Processing Systems (NeurIPS)*, 2025. URL https://arxiv.org/abs/2502.05171.

Alex Graves. Adaptive computation time for recurrent neural networks. *arXiv preprint arXiv:1603.08983*, 2016. URL https://arxiv.org/abs/1603.08983.

Alexia Jolicoeur-Martineau. Less is more: Recursive reasoning with tiny networks. *arXiv preprint arXiv:2510.04871*, 2025. URL https://arxiv.org/abs/2510.04871.

Ferdinand Kapl, Emmanouil Angelis, Kaitlin Maile, Johannes von Oswald, and Stefan Bauer. From growing to looping: A unified view of iterative computation in LLMs. *arXiv preprint arXiv:2602.16490*, 2026. URL https://arxiv.org/abs/2602.16490.

Jonas Knupp, Jan Hendrik Metzen, Jeremias Bohn, Georg Groh, and Kristian Kersting. Depth-recurrent attention mixtures: Giving latent reasoning the attention it deserves. *arXiv preprint arXiv:2601.21582*, 2026. URL https://arxiv.org/abs/2601.21582.

Niru Maheswaranathan, Alex Williams, Matthew D. Golub, Surya Ganguli, and David Sussillo. Reverse engineering recurrent networks for sentiment classification reveals line attractor dynamics. In *Advances in Neural Information Processing Systems (NeurIPS)*, 2019. URL https://arxiv.org/abs/1906.10720.

nostalgebraist. Interpreting GPT: The logit lens. LessWrong blog post, 2020. URL https://www.lesswrong.com/posts/AcKRB8wDpdaN6v6ru/interpreting-gpt-the-logit-lens.

Mitchell Ostrow, Adam Eisen, Leo Kozachkov, and Ila Fiete. Beyond geometry: Comparing the temporal structure of computation in neural circuits with dynamical similarity analysis. In *Advances in Neural Information Processing Systems (NeurIPS)*, 2023. URL https://arxiv.org/abs/2306.10168.

Francesco Pappone, Donato Crisostomi, and Emanuele Rodolà. Two-scale latent dynamics for recurrent-depth transformers. In *NeurIPS 2025 Workshop on Unifying Representations in Neural Models (UniReps)*, 2025. URL https://arxiv.org/abs/2509.23314.

Zirui Ren and Ziming Liu. Are your reasoning models reasoning or guessing? a mechanistic analysis of hierarchical reasoning models. *arXiv preprint arXiv:2601.10679*, 2026. URL https://arxiv.org/abs/2601.10679.

Nikunj Saunshi, Nishanth Dikkala, Zhiyuan Li, Sanjiv Kumar, and Sashank J. Reddi. Reasoning with latent thoughts: On the power of looped transformers. In *International Conference on Learning Representations (ICLR)*, 2025. URL https://arxiv.org/abs/2502.17416.

Amin Sghaier, Ali Parviz, and Alexia Jolicoeur-Martineau. Probabilistic tiny recursive model. *arXiv preprint arXiv:2605.19943*, 2026. URL https://arxiv.org/abs/2605.19943.

Jimmy T.H. Smith, Scott W. Linderman, and David Sussillo. Reverse engineering recurrent neural networks with Jacobian switching linear dynamical systems. In *Advances in Neural Information Processing Systems (NeurIPS)*, 2021. URL https://arxiv.org/abs/2111.01256.

Charlie Snell, Jaehoon Lee, Kelvin Xu, and Aviral Kumar. Scaling LLM test-time compute optimally can be more effective than scaling model parameters. *arXiv preprint arXiv:2408.03314*, 2024. URL https://arxiv.org/abs/2408.03314.

David Sussillo and Omri Barak. Opening the black box: Low-dimensional dynamics in high-dimensional recurrent neural networks. *Neural Computation*, 25(3):626–649, 2013.

Guan Wang, Jin Li, Yuhao Sun, Xing Chen, Changling Liu, Yue Wu, Meng Lu, Sen Song, and Yasin Abbasi Yadkori. Hierarchical reasoning model. *arXiv preprint arXiv:2506.21734*, 2025. URL https://arxiv.org/abs/2506.21734.

Xuezhi Wang, Jason Wei, Dale Schuurmans, Quoc Le, Ed Chi, Sharan Narang, Aakanksha Chowdhery, and Denny Zhou. Self-consistency improves chain of thought reasoning in language models. In *International Conference on Learning Representations (ICLR)*, 2023. URL https://arxiv.org/abs/2203.11171.

## A SYNTHETIC REGRESSION TESTS FOR THE TWO ARTIFACTS

Both methodological artifacts documented in the main text are pinned by synthetic regression tests in our suite; here we describe the constructions and their expected signatures.

**Solve-timing control.** Solve-timing comparisons use solved puzzles to avoid right-censoring cells that never settle. Needs-search cells resolve later in $18/19$ puzzles (one-sided sign test $p = 3.8\times10^{-5}$). Matching on candidate count gives $19/19$ positive differences (two-sided $p = 3.8\times10^{-6}$; Fig. 8); these are distinct tests.

**(a) Mean-field inflation.** We generate a multi-position linear system whose per-position updates share an operator $A$ but carry an independent mean-zero per-position deviation $B_s$, then fit $\Delta z_{t+1} \approx A\,\Delta z_t$ two ways. A single shared operator is the right estimand, and the honest per-position fit recovers it only partly; averaging positions before fitting drives the fit to saturation and raises the complex mass with it. Both inflations reproduce over seeds, in the direction of the empirical jump ($z_L$ $R^2$ $0.43 \to 0.90$, complex mass $\sim0.63 \to \sim0.90$; the honest per-position complex mass is the one that matches the $65\%$ complex fraction of the endpoint Jacobians' retained Ritz values, App. G); the synthetic's *magnitudes* follow its own dimension and are not claimed to match. Two mechanisms travel under one name here. Pooling suppresses position-specific structure by $\sim S^{-1/2}$, and it *also* divides the sample-to-dimension ratio by $S$—here from $\sim$70:1 to under 1:1—so the pooled fit is underdetermined, its in-sample $R^2$ saturates, and its pseudo-inverse manufactures spurious oscillatory modes. The $B_s{=}0$ control lifts the honest fit to the same ceiling, so it cannot assign the $R^2$ inflation to averaging rather than to the collapsed pair count. The synthetic pins the direction of both inflations; it does not separate their causes. Per-position reduction is the correct default for both reasons.

**(b) Under-specified clock.** We construct a three-level-clock scheduled linear dynamical system (a fully *state-independent* program $A(\text{seg}, H, L)$) and condition it on only a coarse phase while treating the pooled-away clock levels as "time." This reproduces the exact false state-dependence signature the coarse-phase test of Sec. 6 returns: low coarse-phase $R^2$ together with high drift-across-time and low drift-across-puzzles. Conditioning on the *full* clock then resolves it ($R^2 \approx 1$, across-puzzle drift $\approx 0$), confirming that the signature is a clock artifact rather than evidence of nonlinearity.

## B CONTROLS FOR OPERATOR DRIFT AND EXPANDING MODES

The even/odd across-puzzle operator drift cannot serve as a state-dependence probe. Each half is a single $\sim$21k-pair fit, and a synthetic well-conditioned null places the estimation floor at $R^2$-scale drift $\sim$0.04–0.17, rising to $\sim$0.6 in the ill-conditioned near-fixed-point regime. The observed drift anti-correlates with per-tick update energy ($\text{corr}(E, \text{drift}) = -0.86$ and $-0.99$ for $z_L/z_H$), exactly the conditioning-driven pattern: the noisiest, lowest-energy ticks inflate drift. We therefore retire drift as a state-dependence signal and rely instead on the split-half held-out $R^2$ of Sec. 6.2 (Eq. 6), which measures fit quality after de-biasing for SNR and conditioning.

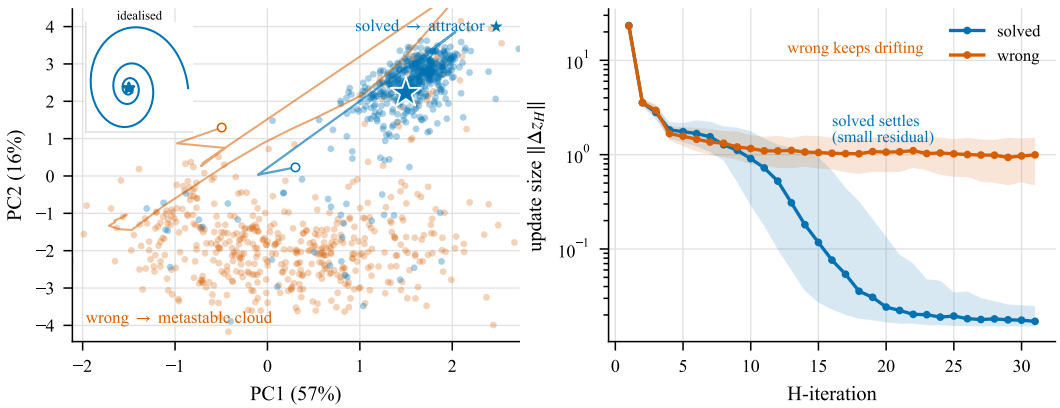


Figure 6: Solved and wrong $z_H$ trajectories. **Left:** the first two PCA components of position-averaged states, shown only for orientation. Neither clustering nor apparent rotation in this projection establishes a fixed point or its stability (App. A). All runs share the learned initial state. **Right:** per-position update norms (median and IQR) decay toward zero for solved trajectories but remain larger for wrong trajectories. Endpoint spectra and answer persistence are measured separately in Secs. 5 and 4.

**The expanding mean-field mode.** A late-window position-mean $z_{\mathrm{ACT}}$ operator yields a spectrally expanding, complex-oscillatory mode (dominant $\lambda = -0.71 \pm 0.89j$, $\rho = 1.14$, $R^2 = 0.94$). It is however *window-fragile*: $\rho$ falls monotonically as the fit window widens ($w$=3 : 1.27, $R^2$ 0.99; $w$=5 : 1.14, 0.94; $w$=7 : 0.89, 0.77; $w$=10 : 0.66, 0.50; $w$=15 : 0.56, 0.37), crossing unity only in the last-third window. The mode is genuinely readout-enriched: its row-space fraction on the 11-dimensional readout is 0.36 against a chance level of 0.021, a 17× enrichment (the $q$-head read fraction is 0.10). But the "confidence-sharpening" attribution does not survive a random-direction null: the mode's margin correlation ($r = 0.69$) sits below the null 95th percentile (0.70), and the net-drift direction correlates more strongly (0.90). We therefore report the enrichment as solid and the sharpening interpretation as *not yet established*.

**Matched perturbation controls.** We perturb along the fitted mode at zero-based injection index 10, after eleven of the 16 segments, with Frobenius norm equal to the median final-segment update. Controls use the same code path: 64 isotropic directions, 24 subdominant eigenvectors of the same operator, and 64 random directions in the top-16 principal subspace of state deltas. The latter two control for alignment with the anisotropic state distribution.

Final-state displacement is 0.055 of the state norm for the mode, versus 0.054 for subspace controls, 0.058 for eigenvector controls, and 0.036 for isotropic controls. The mode's answer-change rate exceeds all isotropic controls on all four tested axes and both signs, but lies at only the 25th–63rd percentile of alignment-matched controls. Its margin effect lies at quantile rank 0.016–0.812 within the matched families and has inconsistent signs across axes. Thus the tested intervention does not support a distinctive confidence-sharpening role, despite readout enrichment. An earlier isotropic-only comparison gave a misleading positive result; regression tests now enforce all three control families.

## C Excluded buckets and conditioning details

**Algorithm 1's *rank* and *filter* steps do not commute**, which is the reason this procedure is written out rather than described. Ranking first and filtering second reports the energetically dominant computation, minus whichever of those ticks cannot be scored reliably, and says which. Filtering first would admit a low-energy but well-conditioned tick into the top-$c$ in its place, so the number would describe a different computation while carrying the same name. Our implementation fixes the order in one place and a unit test pins it; the two orders are not otherwise distinguishable from a reported $R^2_{\mathrm{hi}}$.

Table 1: Full-clock per-tick linear fits (per-position). hi-E is the energy-weighted $R^2$ over the top-tercile ticks (Eq. 5); held-out and $R^2_{\text{corr}}$ are the split-half reliability figures (Eq. 6; $\approx$1 = reliably estimated). The estimator behind every cell, including the order its two selection steps run in, is Algorithm 1. The time-invariant-operator $R^2$ is the first rung of Fig. 1(b) and is quoted in Sec. 6; the raw ceiling enters only through $R^2_{\text{corr}}$, so neither is repeated here.

| stratum | hi-E | **held-out** | $R^2_{\text{corr}}$ | corr$(E, R^2)$ |
|---|---|---|---|---|
| solved $z_L$ | 0.73 | **0.72** | 0.96 | $+0.76$ |
| solved $z_H$ | 0.39 | **0.37** | 0.90 | $+0.03$ |
| unsolved $z_L$ | 0.80 | **0.80** | 0.99 | $+0.80$ |
| unsolved $z_H$ | 0.42 | **0.39** | 0.91 | $+0.88$ |

**Algorithm 1** Full-clock linearity estimate for one (stratum, timescale). $R^2(A; X)$ scores operator $A$ on half $X$; the per-tick loop computes Eq. 6 and the return is Eq. 5. Steps are named rather than numbered because the numbers move when the listing is edited: the listing below is the procedure we ran, and no other.

**Input:** updates $\Delta z_t$, each tagged with its full clock tick $\varphi{=}(s, h, \ell)$ and its puzzle id
**Params:** $c{=}\frac{1}{3}$, $\tau{=}0.3$ (App. F)
**for** each clock tick $\varphi$ **do**
  split puzzles by parity into halves e, o
  accumulate $(C_0, C_1, S_{yy})$ per half; $A_X \leftarrow C_1^X (C_0^X)^+$
  $R^2_{\text{ho}} \leftarrow \frac{1}{2}[R^2(A_{\text{e}}; \text{o}) + R^2(A_{\text{o}}; \text{e})]$
  $R^2_{\text{ceil}} \leftarrow \frac{1}{2}[R^2(A_{\text{e}}; \text{e}) + R^2(A_{\text{o}}; \text{o})]$
  $E(\varphi) \leftarrow \sum_{t\in\varphi} \|\Delta z_t\|^2$
**end for**
$\Phi_{\text{fin}} \leftarrow \{\varphi : R^2_{\text{ceil}}(\varphi)$ finite$\}$
**rank:** $\Phi_{\text{top}} \leftarrow$ the $\max(1, \text{round}(c|\Phi_{\text{fin}}|))$ ticks largest in $E$
**filter:** $\Phi_{\text{use}} \leftarrow \{\varphi \in \Phi_{\text{top}} : R^2_{\text{ceil}}(\varphi) \geq \tau\}$
report the excluded $\Phi_{\text{top}} \setminus \Phi_{\text{use}}$
**return** $R^2_{\text{hi}} = \sum_{\Phi_{\text{use}}} E R^2_{\text{ho}} / \sum_{\Phi_{\text{use}}} E$

Full-clock buckets whose de-biased ceiling falls below 0.3 are excluded from the headline hi-energy fits. These are the low-energy, near-fixed-point ticks: once the trajectory has contracted, per-tick updates are dominated by noise and the fit is ill-conditioned, so any $R^2$ there reflects estimation error rather than dynamics. The retained buckets are well-specified: each full-clock operator on a full stratum is estimated from 41,984 update vectors (512 puzzles $\times$ 82 positions), 82 observations per predictor. The held-out operators of Eq. 6 are each fitted on one parity half, 20,992 vectors, so their ratio is 41 : 1. As a correctness check, the streaming second-moment estimator agrees with a direct fit on the held full trajectories to $\max|\Delta R^2| = 1.1 \times 10^{-14}$, confirming that streaming introduces no numerical bias.

## D Input-conditioned and nonlinear refits

The fast-loop linearity claim (Sec. 6) faces one alternative: the L-module is fed the injection $z_H{+}x$ each step, so a per-tick operator could be absorbing that exogenous linear input rather than performing genuine recurrent dynamics. We test this directly. Each full-clock tick is refit jointly on the previous update and the injection,

$$\Delta z_{t+1} \approx A_\phi \, \Delta z_t + B_\phi \, (z_H{+}x) + c,$$

and we score three nested sub-models held-out across a puzzle-parity split (fit on even-indexed puzzles, score on odd, and vice versa): state-only $[\Delta z_t,\ 1]$, injection-only $[z_H{+}x,\ 1]$, and full $[\Delta z_t,\ z_H{+}x,\ 1]$. All three carry the intercept $c$, so the state-only sub-model is affine and is not the through-origin fit of Sec. 6.2. The operator's *unique* held-out gain is $\Delta_{\text{op}} = R^2_{\text{full}} - R^2_{\text{inj}}$, the variance the recurrent operator explains that the injection cannot; symmetrically $\Delta_{\text{inj}} = R^2_{\text{full}} - R^2_{\text{state}}$. Held-out scoring is essential: adding the injection block can only inflate the in-sample fit, so the sign of $\Delta_{\text{inj}}$ is meaningful only out of sample.

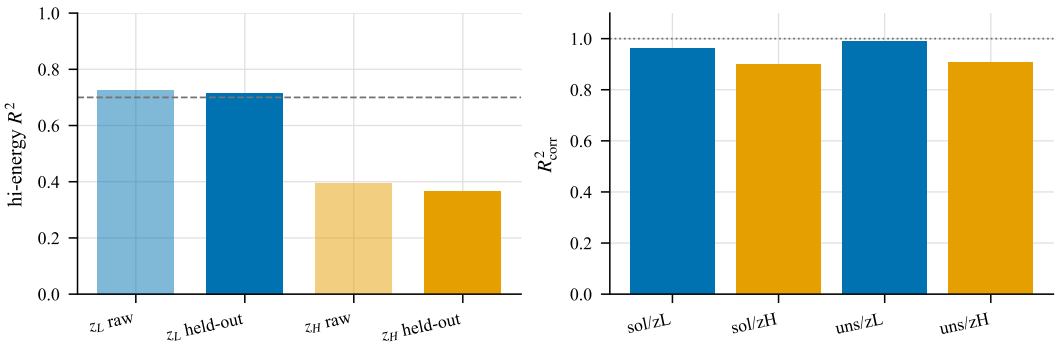


Figure 7: Split-half reliability (Sec. 6). **Left:** raw vs. held-out hi-energy $R^2$ for $z_L/z_H$: the fast/slow gap survives the correction (held-out 0.72 vs. 0.37, a $+0.35$ gap). **Right:** $R^2_{\text{corr}}$ per timescale and stratum ($\approx$1 = reliably estimated).

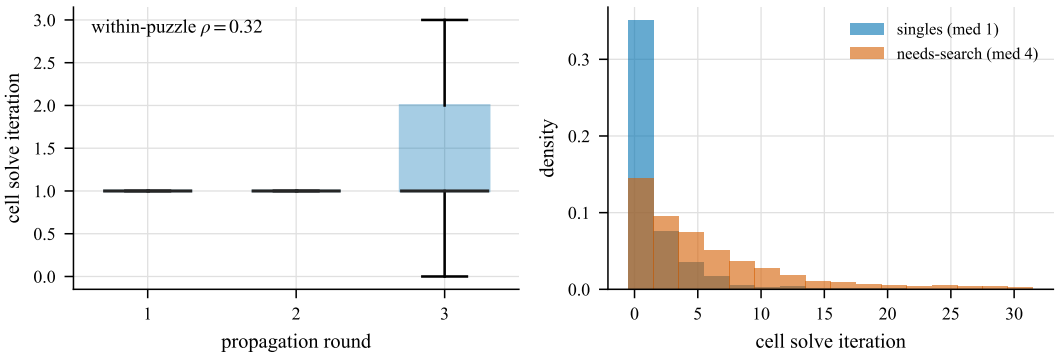


Figure 8: Constraint-propagation grounding (solved stratum). Cell solve-time tracks naked/hidden-singles propagation depth (within-puzzle Spearman $\rho$=0.32); search-requiring cells resolve later than singles-determined ones (mean iteration 6.3 vs. 2.1, Mann–Whitney $p$ below reported numerical precision). The obvious objection is that search-requiring cells are simply *harder*; matching cells on their surviving-candidate count within each puzzle leaves the gap at $+2.7$ segments ($19/19$ puzzles positive, two-sided exact sign test $p$=$3.8 \times 10^{-6}$; the unmatched comparison App. A quotes is a different, one-sided test at $18/19$), and a cell-level ANCOVA over 1,740 cells gives the needs-search indicator $+2.26$ segments against $+0.12$ per additional candidate. Its standard errors, 0.15 and 0.06, are ordinary least squares over cells and treat the cells of one puzzle as independent, so they are narrower than a puzzle-clustered interval. Difficulty is real and small; it is not what the fingerprint is tracking. Only 20.9% of solved puzzles are fully singles-determined; the model resolves 19,352 cells the propagator cannot.

Table 2 reports the three most energetic $z_L$ ticks on the stratified 1024-puzzle sample. At the top two, adding the injection changes held-out $R^2$ by $-0.003$: it adds no predictive information given the previous update. At the third, lower-energy tick, it improves prediction. This pattern occurs in both strata; no comparable operator dominance appears for $z_H$. Predictor redundancy does not establish that the drive is causally irrelevant.

**Nonlinear refits recover little beyond the linear fit.** To test whether $z_H$'s low per-tick linear $R^2$ reflects a *recoverable* nonlinearity or genuine complexity/noise, we refit the same per-tick, per-position problem ($\Delta z_{t+1} = g(\Delta z_t)$) on the top-tercile energy ticks with two nonlinear classes: RBF kernel ridge (Nystrom, $\sim$2048 landmarks) and a 512$\rightarrow$1024$\rightarrow$512 GELU MLP (early-stopped on a validation split), under the same split-half (puzzle-parity) protocol as Table 1 but aggregated over *all* top-tercile ticks (no reliability-ceiling exclusion) and fit on a capped per-tick pair reservoir, so all three classes see identical pairs; this lowers the absolute linear baseline relative to Table 1 (read within-row; see the Table 3 caption). Both lift $z_H$ by only $\approx$0.03 held-out $R^2$ over linear, comparable to their gain on $z_L$, and neither approaches a good fit. The method is not at fault: on a synthetic

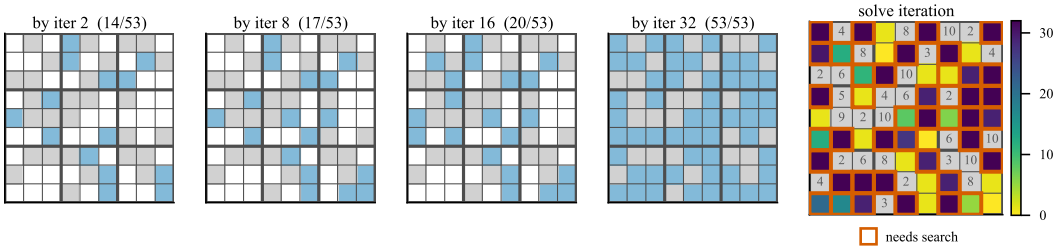


Figure 9: **One solved Sudoku (illustrative). First four panels:** cumulative solve-time wavefront: a cell is filled once the H-lens fixates it correctly by iteration $t$ (count shown); a core resolves early, the rest commit late. **Right:** the same board coloured by solve iteration (light early, dark late), with needs-search cells (no naked/hidden single; red outline) tending to resolve later than singles-determined ones, the single-puzzle view behind the aggregate $\rho$=0.32 of Fig. 8.

Table 2: Injection-conditioned refit at the three most energetic $z_L$ ticks (held-out $R^2$; ticks ordered by update energy). $\Delta_{\text{op}}$ is the operator's unique gain over the injection, $\Delta_{\text{inj}}$ the injection's over the operator. At the two dominant ticks the injection adds nothing ($\Delta_{\text{inj}} \approx 0$).

| stratum | tick | state | inj | full | $\Delta_{\text{op}}$ | $\Delta_{\text{inj}}$ |
|---|---|---|---|---|---|---|
| solved | 1 | 0.872 | 0.730 | 0.868 | +0.138 | −0.003 |
| solved | 0 | 0.951 | 0.898 | 0.948 | +0.050 | −0.003 |
| solved | 2 | 0.625 | 0.807 | 0.818 | +0.010 | +0.193 |
| unsolved | 1 | 0.873 | 0.729 | 0.869 | +0.140 | −0.003 |
| unsolved | 0 | 0.951 | 0.898 | 0.949 | +0.050 | −0.003 |
| unsolved | 2 | 0.664 | 0.820 | 0.829 | +0.010 | +0.165 |

*state-dependent* generator it recovers +0.27 over linear, and on the scheduled-*linear* control (App. A) it correctly recovers ≈0. The residual therefore remains poorly predicted by these particular kernel and MLP fits. Reproducible held-out performance reduces concern about estimation error in the fitted operators, but does not distinguish unobserved inputs, stochastic variation and more complex nonlinear structure.

Table 3: Held-out $R^2$ of per-tick refits on the top-tercile energy ticks (same split-half protocol as Table 1). Nonlinear classes barely exceed linear on the real data; the synthetic controls confirm the method's sensitivity. **Read within-row.** The *linear* column is lower than Table 1's held-out hi-E ($z_L$ 0.55 vs. 0.72; $z_H$ 0.12 vs. 0.37) for two reasons, both applied identically to all three classes: (i) this tercile mean retains *all* top-tercile ticks, whereas Table 1 additionally drops ticks whose split-half reliability ceiling is $< 0.3$ (near-fixed-point, rank-collapsed), the dominant factor ($z_L$ 0.72→0.58, $z_H$ 0.37→0.20); and (ii) each operator here is fit on a capped $\leq$ 16,000-pair/tick reservoir ($z_L$ 0.58→0.55, $z_H$ 0.20→0.12). The linear-vs-nonlinear gap *within* this table is unaffected.

| | linear | kernel | MLP |
|---|---|---|---|
| solved $z_L$ | 0.55 | 0.56 | 0.57 |
| solved $z_H$ | 0.12 | 0.14 | 0.16 |
| unsolved $z_L$ | 0.55 | 0.56 | 0.57 |
| unsolved $z_H$ | 0.17 | 0.18 | 0.20 |
| scheduled-LDS (control) | 0.84 | 0.84 | 0.84 |
| state-switch (positive) | 0.65 | 0.90 | 0.92 |

## E STEP SIZE AND MATCHED TEMPORAL GRANULARITY

A fair objection to the timescale split is that the two streams are not on the same footing: $z_L$ takes four updates per segment under a drive held constant within an H-cycle, $z_H$ two. A finer timestep buys higher one-step predictability for purely kinematic reasons, so the split could be a coarse-graining

artifact rather than a statement about computation. Split-half correction de-biases estimation noise and App. D rules out the injection as the predictor; neither addresses this.

The natural control is to plot per-tick $R^2$ against *relative* step size $\|\Delta z\|/\|z\|$ and ask whether the two streams fall on one curve. That control is unavailable in this architecture, for a reason worth stating rather than discovering twice: the blocks are post-norm with RMSNorm, so $\|z\|$ is pinned. Measured across every recorded tick of both streams, the median state norm is $22.63$ with a coefficient of variation of $0.000$. Relative step size is therefore a constant rescaling of absolute step size—the rank correlation between them is exactly $+1.000$—and normalising by $\|z\|$ cannot separate anything.

What can still be said without it: on a single estimator (median per-tick $R^2$ over the solved stratum), restricting both streams to their overlapping step-size range moves the gap from $+0.060$ to $+0.050$, i.e. the ordering does not come from $z_L$ occupying a gentler part of the step-size axis.

**The composition control, run.** The sharper control is to remove the granularity difference outright: sample $z_L$ only at H-cycle boundaries, so differencing yields one *composed* update per (segment, H-cycle) instead of $L$ one-step updates. The composed stream ($z_L^{\mathrm{c}}$) then occupies $z_H$'s clock grid exactly—30 *fittable* buckets each, of the 31 ticks that grid has—and every downstream step, split-half halves, high-energy weighting, held-out scoring and the $0.3$ reliability floor, applies unchanged. *Fittable* is not *reliable* in this paper's sense, and the gap between the two is large enough to state: Algorithm 1 ranks those 30 down to a top tercile of 10, and the floor then filters 8 of those out, so each slow-grid stream reaches the aggregate with the $n{=}2$ the table reports. Everywhere else here, "reliable" counts buckets that survive both steps.

| stratum | $z_L$ (one-step) | $z_L^{\mathrm{c}}$ (composed) | $z_H$ |
|---|---|---|---|
| solved | $0.72$ ($n{=}11$) | $0.59$ ($n{=}2$) | $0.37$ ($n{=}2$) |
| unsolved | $0.80$ ($n{=}5$) | $0.63$ ($n{=}2$) | $0.39$ ($n{=}2$) |

The split survives: at matched granularity the solved-stratum gap is $+0.22$ ($0.59$ vs. $0.37$), so the fast loop is more linear than the slow one for reasons that are not the clock. But the control is not free, and we state its cost rather than only its verdict. Composition removes $37\%$ of the headline gap ($+0.35 \to +0.22$; $41\%$ on unsolved), so a substantial minority of the reported split *was* granularity. And the composed estimate inherits $z_H$'s scarcity—$n{=}2$ reliable high-energy buckets, because fewer, larger updates survive the reliability floor less often—so it is a two-bucket comparison of the kind we flag elsewhere in this paper. The claim we take from it is the ordering, not the size.

**What a position-wise operator cannot represent.** A second objection reaches further. Each operator is a single $512\times512$ map fitted per clock tick on update vectors pooled over puzzles *and* positions, so it carries no term by which position $i$'s update depends on position $j$'s state. The model, being a transformer, mixes positions at every block through self-attention. A position-wise fit can absorb cross-position effects to the extent that they are linearly predictable from the local update; effects it cannot predict contribute to the residual. Thus "poorly linearisable" cannot be read as "nonlinear in its own state".

Using the same estimator for both streams does not remove this limitation: differences in the strength or local predictability of cross-position effects can affect the fast–slow $R^2$ ordering. The association with constraint propagation in Sec. 7 is compatible with such an explanation, but does not distinguish it from other sources of prediction error.

Testing this explanation would require a cross-position predictor evaluated under the same held-out protocol, checking whether the fast–slow $R^2$ gap narrows. We did not fit one. Until it is fitted, the supported statement is the one Sec. 9 makes: low held-out $R^2$ is limited prediction by the tested families, not a mechanism and not irreducible nonlinearity.

## F Sensitivity to energy and reliability thresholds

Two hyperparameters were fixed by hand: a reliability-ceiling floor of $0.3$ and a top-third energy cut. Both enter the same aggregate, so we sweep them—floor $\in \{0.2, 0.3, 0.4\}$ $\times$ fraction $\in \{0.2, \frac{1}{3}, 0.5\}$

$\times$ {energy-weighted, unweighted}, 18 cells per setting, on the solved stratum. Nothing about the estimator changes; only what it is asked.

| setting | cells | gap min | median | flips |
|---|---|---|---|---|
| HRM seed 0 | 18 | $+0.107$ | $+0.350$ | 0 |
| HRM seed 1 | 12 | $+0.074$ | $+0.232$ | 0 |
| composed $z_L^c$ | 18 | $+0.049$ | $+0.157$ | 0 |
| TRM ($N$=4096) | 18 | $-0.143$ | $+0.080$ | 2 |

("gap" is fast minus slow held-out hi-energy $R^2$; a cell is unscorable when a threshold empties one side, which is why seed 1 has 12.)

**Reliable-tick coverage.** At floor 0.2 and top-half energy selection, the slow stream retains 14 ticks on seed 0 and 10 on seed 1; the gaps remain 0.37 and 0.26. Relaxing the floor alone increases the counts from 2 to 9 and from 1 to 5, respectively. Sparse coverage under the default settings therefore depends on both thresholds.

**TRM sensitivity.** Two of TRM's eighteen solved-stratum cells have negative gaps ($-0.02$ and $-0.14$, both unweighted). This is consistent with the absence of a solved split at $N = 4096$ ($0.48/0.48$); this sweep does not test the reported unsolved-stratum inversion.

## G SCALED ENDPOINT JACOBIAN SPECTRA

The Sec. 5 measurement draws 256 solved and 256 wrong terminal states (wrong sampled proportionally across the 1–5/6–20/$>$20 wrong-cell buckets, $85/85/86$), all through the same endpoint-Jacobian JVP + $m$=40 Arnoldi estimator; only per-example scalars are kept (no traces). Here and in the legacy figure labels, $\rho$ abbreviates the estimated leading-Ritz radius $\hat{\rho}_{40}$, not a certified full spectrum. Fig. 11 shows the retained Ritz values themselves in the complex plane, which the main-text distribution summarises away. The $n$=16 pilot behind its first three panels replicates at scale: solved $f_H$ contracts (mean $\rho$=0.44, gate-passing max 0.82, 65% complex; the 3 solved states above 0.9 all fail the terminal-update gate), wrong $f_H$ spreads higher (mean 0.75, median 0.77), with 9.4% above 0.9 and 2.7% with an estimated expanding leading mode ($\hat{\rho}_{40}>1$; $7/256$, 95% Wilson CI $[1.3, 5.5]$%), so the expanding-mode estimate recurs across several examples rather than one outlier (Fig. 10). Neither tail is reported without the other. Raw, the two classes both have one: $2/256$ solved endpoints exceed unity and the single largest radius in the whole dataset (1.32) is a solved state, above the wrong-class maximum of 1.17. Gated to the terminal-update criterion the picture is one-sided, because both solved outliers fail that gate: $0/243$ gated solved endpoints exceed unity (max 0.82) against $4/176$ gated wrong ones (max 1.17, itself a gate-passing endpoint). This is the same gate the TRM comparison in App. V applies, and the reason the main text prefers AUC=0.913 over either tail as the class summary. Written once, the gate of Sec. 3 is

$$\begin{aligned} \mathrm{gate}(i) &= \Big[\ \|\Delta z_i^{\mathrm{final}}\|/\|z_i\| \ \le\ q_{95}\ \Big], \\ q_{95} &= \mathrm{pctl}_{95}\Big\{\|\Delta z_j^{\mathrm{final}}\|/\|z_j\|\Big\}_{j\ \mathrm{solved}}, \end{aligned} \tag{7}$$

and every gated number in this paper—here, App. R, App. V, App. H—is this expression with the solved class of its own setting supplying $q_{95}$. Calibrating on the solved class, rather than on an absolute tolerance, is what lets one gate travel between architectures and tasks whose state norms differ; it also means 95% of solved endpoints pass by construction, so the gate is only ever informative about the wrong class. 69% ($176/256$) of wrong endpoints clear it vs. 95% of solved; wrong-state estimated leading-Ritz radius correlates only weakly with failing that gate ($r$=0.22). Within the wrong class that tail sits in the *mildest* bucket ($5/85$ at 1–5 wrong cells, versus $1/85$ at 6–20 and $1/86$ at $>$20; max $\rho$=1.17)—the opposite of a severity-tracks-instability reading, consistent with the small-step-but-wrong mild-failure regime of Sec. 4, and a further reason the 2.7% is reported as a distributional tail rather than as a mechanism.

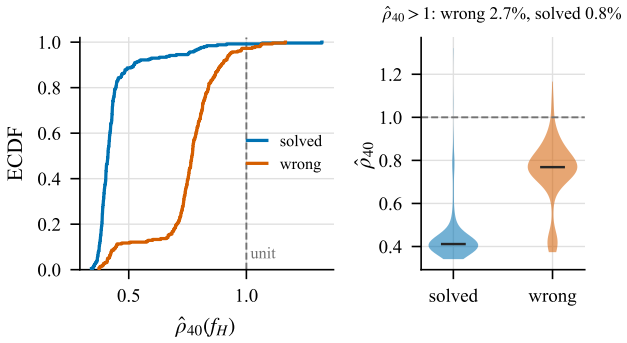


Figure 10: Endpoint $f_H$ leading-Ritz radius, 256 solved endpoints vs. 256 wrong terminal states (AUC=0.913). **Left:** ECDF, unit line dashed. **Right:** violin by class; the tail past one is a distributional property ($7/256$ wrong, $2/256$ solved), not one outlier. Per-example complex-plane spectra: App. Fig. 11.

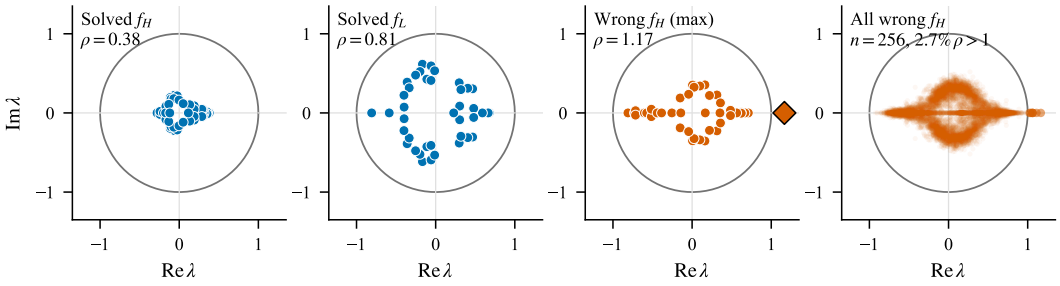


Figure 11: Endpoint Jacobian Ritz values ($m = 40$ Arnoldi; unit circle shown). **Panels 1–2:** representative solved $f_H$ and $f_L$ spectra ($\hat{\rho}_{40} = 0.38, 0.81$). **Panel 3:** the largest wrong-$f_H$ estimate (1.17). **Panel 4:** all 256 wrong-$f_H$ spectra. Estimates exceed one for $7/256$ wrong and $2/256$ solved endpoints; after the terminal-update gate, the counts are $4/176$ and $0/243$. These are local linearisation estimates; a stability or saddle interpretation additionally requires an appropriate fixed point.

## H Replay-label consistency and weighted sampling

Every stratified analysis here pairs a solved/wrong label taken from the *frozen evaluation dump* with a state the analysis *replayed itself*. Our reproducibility statement records that the instrumented loop matches the training forward pass to `bfloat16` tolerance; what it did not record is how many endpoints live inside that tolerance. We measured it, because an endpoint whose replay decodes differently from the dump is analysed under a label that does not describe it.

**How often the two disagree.** Re-decoding each replayed endpoint and comparing to the dump gives $467/512$ agreement overall, and the disagreement is strongly asymmetric across severity:

| dump stratum | agree (batch 1) | $n$ | agree (batch 128) | $n$ |
|---|---|---|---|---|
| solved | 0.953 | 256 | 0.957 | 512 |
| wrong 1–5 | **0.722** | 90 | **0.741** | 170 |
| wrong 6–20 | 0.919 | 86 | 0.947 | 170 |
| wrong >20 | 0.988 | 80 | 0.983 | 172 |

The two columns are separate draws, not the same endpoints replayed twice, so their agreement bounds how large a batch-composition effect could be rather than excluding one. Within each, the effect is that endpoints one or two cells from correct sit inside the `bfloat16` tolerance, and 27.8% of the mild bucket re-decodes as fully solved. Concordance is now emitted by every basin run.

**Re-indexing the rates by the state actually analysed.** Relabelling moves 45 of 512 endpoints across the solved/wrong split and at least 70 across the four severity buckets; the mild bucket loses more than half its members—not only the 25 that become solved, but others whose replay error count exceeds five. The paper's contrast *widens* under the more self-consistent labelling:

| | dump label (this draw) | | replay label | |
|---|---|---|---|---|
| class | $R_{\text{ans}}$ | $n$ | $R_{\text{ans}}$ | $n$ |
| solved | $0.953\,[0.93, 0.98]$ | 256 | $0.993\,[0.98, 1.00]$ | 277 |
| wrong 1–5 | $0.400\,[0.31, 0.50]$ | 90 | $0.325\,[0.18, 0.47]$ | 40 |
| wrong 6–20 | $0.128\,[0.06, 0.20]$ | 86 | $0.041\,[0.01, 0.08]$ | 98 |
| wrong >20 | $0.025\,[0.00, 0.06]$ | 80 | $0.010\,[0.00, 0.03]$ | 97 |

**Reporting rule and sampling limitation.** The relabelled groups inherit unequal inclusion probabilities from the dump-stratified draw; their unweighted rates are conditional on that draw. The mild group also shrinks to $n$=40, with a wide interval. We retain the original dump-labelled headline for consistency with TRM and Maze, and report replay labels as a sensitivity analysis. The job script specified before execution that the headline would be retained if the replay-mild upper confidence bound remained below $\frac{1}{2}$ and disjoint from the solved interval. This condition held.

This draw is separate from the larger replication in App. M, whose 512 solved and 170 mild-wrong endpoints supply the main-text rates. Subsequent basin runs emit both labellings. The probability-sampling audit below addresses the unequal-inclusion issue directly.

**Sampling on the replay label, rather than relabelling after the draw.** The objection above is a design defect, not a presentation one: no reordering of an already-drawn sample fixes it. So we redrew. Every valid test example is assigned its dump stratum, the 934-example mild stratum is taken as a *census* and the other three at known rates ($4000/176{,}574$ solved, $2000/47{,}142$, $2000/198{,}136$), each drawn example is replayed once at batch size 1, and the sample is stratified on what that replay *decodes to*. Inclusion probabilities are known by construction, and the class rates are inverse-probability weighted, $\hat{R}_C = \sum_i w_i \mathbf{1}[C_i{=}C] r_i / \sum_i w_i \mathbf{1}[C_i{=}C]$ with $w_i = 1/(\pi_{1i}\pi_{2i})$. The draw has two stages: the 8934-example screen above is stage 1, and stage 2 takes the 1952 endpoints the sweep perturbs, 512 per replay stratum except mild, where only 416 were available and all were taken. This is the Hájek ratio form, which corrects for the unequal inclusion probabilities and is design-consistent for the frame; it is not finite-sample unbiased, and we do not claim it is. Within a class $\pi_{2i}$ is constant, so it cancels from $\hat{R}_C$ but not from any population total. Intervals resample endpoints within each design stratum. A uniform draw was rejected on measurement: the design's own Horvitz–Thompson estimate puts the replay-mild population at 845 of 422,786 examples (0.200%; the dump-mild stratum is 934, 0.221%), so landing $n$=170 replay-mild that way needs ∼85,000 replays against this design's 8934. Every endpoint re-decoded to the label the sampler had assigned it ($1952/1952$), so the replay is deterministic and the probabilities describe the endpoints they are attached to.

| class | dump-drawn (published) | replay-drawn, IPW/Hájek |
|---|---|---|
| solved | $0.953\,[0.934, 0.971]$ | 1.000 |
| wrong, 1–5 | $0.418\,[0.347, 0.494]$ | $\mathbf{0.178}\,[0.156, 0.201]$ |
| wrong, 6–20 | $0.088\,[0.047, 0.135]$ | $0.020\,[0.009, 0.033]$ |
| wrong, >20 | $0.041\,[0.017, 0.076]$ | $0.064\,[0.043, 0.087]$ |

Rates are $R^{(C)}_{\text{ans}}(0)$, with $n = 512/416/512/512$. The solved–mild separation widens: 3.5% of dump-solved endpoints replay as wrong, while 30% of dump-mild endpoints replay as solved, inflating the dump-mild persistence rate. Three qualifications remain. The observed solved rate of 1.000 has a degenerate bootstrap and is not evidence of zero population uncertainty. Severity is no longer monotone: the 6–20 bucket lies below the $> 20$ bucket on disjoint intervals. Mild remains the most persistent wrong bucket. Finally, the headline retains dump labels for cross-setting consistency; the replay-weighted audit establishes robustness of the separation, not equivalence of the two estimands.

**Does anything *else* in the paper depend on the labelling? A post-hoc sensitivity check.** The redraw above repairs the stationarity result, which is the one the headline rests on. Two other

results are label-dependent and were not redrawn: Sec. 5's endpoint spectral separation and Sec. 4's probe-versus-q-halt comparison, both computed on the *dump*-stratified $512{+}512$ sample. Redrawing them would mean re-running the Arnoldi estimator on a new probability sample, which we did not do. Instead we relabel the endpoints already measured, using the terminal H-lens decode the instrumented forward pass had already recorded ($\hat{y} = \arg\max \mathrm{lm_head}(z_H)$ at the last H-step), so no new forward pass is needed. **This is a post-hoc sensitivity analysis, not a replacement estimator**: the sample was drawn stratified on the dump label, so a replay-label group is whatever fell into it rather than a stratified sample of its class—the same design objection this appendix raises against the relabel-after-the-draw table above, and the reason the redraw exists. Nothing below changes a reported number. On this draw the two labellings agree on $83.1\%$ of severity buckets and on $92.4\%$ of the solved/wrong split, with the disagreement concentrated in the same place as before ($95.7\%$ agreement on solved, $41.2\%$ on mild, of which $25.9\%$ replay as fully solved).

*The spectral separation does not depend on the labelling.* On the same $512$ endpoints, the leading-Ritz AUC moves from $0.913\,[0.886, 0.940]$ under the dump label ($256/256$) to $0.928\,[0.902, 0.953]$ under the replay label ($275$ solved / $237$ wrong); a paired bootstrap over the relabelled endpoints puts the shift at $+0.014\,[-0.011, +0.039]$, an interval containing zero. Only $37$ of $512$ endpoints move class ($28$ wrong→solved, $9$ the other way), and restricting to the $475$ on which the two labellings agree gives $0.950$. The expanding tail is untouched in its numerators—the same $7$ wrong and $2$ solved endpoints exceed unity under either label; only the denominators shift, so the wrong-class rate reads $2.7\%$ or $3.0\%$. One detail *is* label-sensitive and we flag it: the strict one-sidedness after gating ($0/243$ solved vs. $4/176$ wrong) survives relabelling under the published gate ($0/257$ vs. $4/162$), but if $q_{95}$ in Eq. 7 is instead recomputed over the *replay*-solved residuals it becomes $1/261$ solved against $6/216$ wrong. The tail stays roughly six times more common among wrong endpoints, but "zero on the solved side" is a property of the published gate rather than a label-independent fact.

*The probe comparison survives, and strengthens.* Absolute AUROCs are not comparable across the two labellings here, and the reason is worth stating rather than working around: the replay label is a deterministic function of the same terminal $z_H$ that both the probe and the q-halt head read, so relabelling inflates *both* scores towards $1$ (probe $0.993$, q-halt $0.995$ overall). What the paper's claim rests on is the *gap*, and the gap is what to compare. Under the dump label the probe beats q-halt by $+0.006$ overall and $+0.012$ on the mild bucket; under the replay label it does not beat it at all ($-0.002$ and $-0.014$). Sec. 4's conclusion—that correctness is not substantially more linearly decodable than the halting head already extracts—is therefore understated as published, not overstated, on either labelling. The dump-label column reproduces Sec. 4's $0.941$/$0.887$ to within $0.002$ under a different scikit-learn build; we quote the published values in the body.

**Every setting, at its own published configuration.** Everything above concerns Sudoku/HRM. The other five settings reported dump-labelled rates with nothing to compare them against, so each published sweep was re-run at its own checkpoint, sample, seed, endpoints-per-class and wrong strata, with the radius list truncated to that setting's headline radius plus the $\varepsilon{=}0$ control. The perturbation seed is a function of (endpoint, radius, seed) alone, so the surviving radius is unchanged and the dump column has to reproduce the published number. It does, in all five settings that have a published counterpart. Seed $1$ was instead re-run at seed $0$'s configuration, which makes the two seeds severity-comparable for the first time and leaves it without such a check.

| | | solved $R_{\mathrm{ans}}$ | | wrong $R_{\mathrm{ans}}$ | | gap |
|---|---|---|---|---|---|---|
| setting | concordance | dump | replay | dump | replay | change |
| HRM · Sudoku, seed 0 | 0.918 | 0.954 | 0.992 | 0.181 | 0.072 | +0.15 |
| HRM · Sudoku, seed 1 | 0.892 | 0.918 | 0.971 | 0.147 | 0.033 | +0.17 |
| TRM · Sudoku | 0.818 | 0.958 | 1.000 | 0.323 | 0.000 | +0.37 |
| HRM · Maze | 0.833 | 0.599 | 0.755 | 0.301 | 0.258 | +0.20 |
| HRM · N-Queens 10×10 | 0.953 | 0.958 | 1.000 | 0.559 | 0.532 | +0.07 |
| TRM+GRAM · N-Queens | 0.969 | 0.983 | 0.967 | 0.835 | 0.847 | −0.03 |

Wrong-class rates pool the severity buckets the setting drew from. Concordance is below $1$ everywhere and the disagreement is never symmetric. Maze is the extreme: $28\%$ of its dump-solved endpoints replay as wrong, which is most of what its weak published separation was. The solved-minus-wrong gap widens in five of the six and narrows only for the GRAM-guided recurrence, the setting with the

highest concordance and so the least room to move. The ordering solved $>$ wrong holds $6/6$ under either label. Dump labelling was understating the separation rather than manufacturing it, which is the same direction the Sudoku redraw above found.

*What a replay bucket means on a multi-solution task.* The replay severity code counts cells differing from the *canonical* board, so on N-Queens a replay-mild endpoint may be a different valid solution rather than a near-miss. The solved/wrong split is unaffected—both labels mean "exactly canonical"—but the two N-Queens rows' replay *buckets* are distance from the canonical board, not severity of failure.

*How exactly these reproduce.* The TRM re-run first missed its published counterpart by exactly one endpoint per class, with a perturbation scale of $14.13$ against the published $10.82$, on the same seed, sample and code. The published run used an L40S and the re-run an RTX 6000 Ada; TRM does not contract at the horizon ($\|\Delta z_H\|/\|z_H\| \approx 0.11$), so a different floating-point reduction order moves $z^*$ and with it the median one-step displacement that sets the noise amplitude. Repeating the re-run on an L40S returns $10.82$ and the published rates exactly, and the GRAM setting, re-run on the same device as its published counterpart, reproduced its scale to six digits throughout. The table reports the L40S run. Reproduction of any rate here is therefore good to about one endpoint per class across devices, and we do not claim more.

**"The wrong class" is not the same estimand twice.** Each setting reports one wrong-class rate and the six are read side by side, but each is a mixture over severity and the mixtures are set by whichever binds first, the sampler's cap or the pool itself. In the test frame, mild failures are $0.4\%$ of Sudoku's wrong endpoints ($934$ of $246{,}212$), $2.4\%$ of seed 1's, $0.2\%$ of TRM's ($10$ of $6{,}591$) and $13.4\%$ of Maze's ($120$ of $893$); the two N-Queens settings have no mild wrong bucket at all, because there stratum 1 is a valid answer and the wrong class is drawn from the invalid strata only. In the analysed samples the caps invert part of that: mild is a third of Sudoku's wrong class and a quarter of Maze's, but $1\%$ of TRM's and none of the GRAM run's, whose $64$ wrong endpoints are $95\%$ severe. So the settings' wrong-class levels average over compositions ranging from a third mild to none, which is a second reason—independent of the per-run $\kappa$ of Sec. 9—that the levels are not comparable across settings while the within-setting ordering, measured on one draw under one protocol, is.

## I PRE-SPECIFIED AND EXPLORATORY ANALYSES

Thirteen of the $63$ job scripts carry a literal `PRE-REGISTERED READ` tag, $14$ occurrences in all: $13$ distinct rules, since `rans_interval` and `rans_severity` share one verbatim and one script carries two. A fourteenth, the replay sampler, carries a separate `PRE-COMMITTED READ` rule. These are internally *pre-specified*, not externally preregistered. The original endpoint and timescale analyses are exploratory; the table distinguishes their follow-up tests from post-hoc checks.

| claim / analysis | status | the rule, and which branch fired |
|---|---|---|
| *Confirmatory: a rule was fixed and committed before the run.* | | |
| Wrong answers are non-stationary (Sec. 4) | pre-specified | Stands only if solved and mild intervals are disjoint and mild's upper end stays below $\frac{1}{2}$. $0.953$ vs $0.418\,[0.347, 0.494]$: it did. |
| Replay-label audit (App. H) | pre-specified | Keep the dump-labelled headline if the separation survives. It survived on the replay-first probability sample the rule names ($0.178\,[0.156, 0.201]$ vs $1.000$); we kept it. |
| Horizon (App. N) | pre-specified, twice | The first read allowed "wrong states do reach an attractor, merely slowly"—the largest correction available to this paper. It did not fire ($0.43$, no trend, through $2048$ segments). |
| Near-losslessness of the $z_H$ site (Sec. 8) | pre-specified, *overtaken* | Separating Wilson intervals would leave the claim standing; overlapping ones would retire it on power grounds. They separated *against* it ($z_H$ regresses $2.5\times$ as often). That branch was not written down, and we retired the claim anyway. |

| claim / analysis | status | the rule, and which branch fired |
|---|---|---|
| Granularity control (App. E) | pre-specified | Survives at gap $\geq 0.20$, dies at $\leq 0.10$, report the residual in between. It cleared by $0.02$ ($+0.22$), and we wrote it up as the in-between branch. |
| TRM inversion (App. V) | pre-specified | At $N{=}4096$: adequate slow-tick coverage would remove the caveat. The slow cell remained $n{=}2$; the caveat remains. This does not prove larger samples cannot improve coverage. |
| Noise vs. a task-specific baseline (App. J) | pre-specified | Interval covering zero $\rightarrow$ noise adds nothing over symmetry. It did not: $+0.51\,[+0.29, +0.73]$, $21/0$. The gain is real and small. |
| Maze to competence (App. S) | pre-specified | The original rule treated no improvement beyond $10.7\%$ as evidence against training length. The run had median $13\%$, peak $27\%$, below the $40\%$ competence target; the causal inference is unsupported. |
| N-Queens null (App. Q) | pre-specified | The rule contrasted a data-regime null with task specificity. Matched-size Sudoku reached $4.3\%$; cross-task differences prevent isolating a task-specific cause. |
| Maze endpoint spectra (App. R) | pre-specified | Third branch named in advance: a solved class too small to decide $\rightarrow$ report underpowered, do not spend a second run. It fired, on all $107$ solved mazes. |
| Seed-1 full-clock cell (Fig. 15) | pre-specified; later refit | The original run omitted the promised reliable-bucket counts. A later stored refit reports $11$ fast and $1$ slow bucket on solved states; the slow-loop estimate remains sparsely supported. |
| *Exploratory or post-hoc: no rule was fixed in advance.* | | |
| Endpoint Jacobian spectra (Sec. 5) | exploratory | The original measurement pipeline; the confirmatory work above tests what it found. |
| The timescale split itself (Sec. 6) | exploratory | Discovered, not predicted. Its controls were pre-specified; the finding was not. |
| Threshold sensitivity (App. F) | post-hoc | Run to answer the $n{=}1$–$3$ objection after it was raised. |
| Replay-label sensitivity of spectra and probe (App. H) | post-hoc | Asks whether anything *other* than the stationarity result moves under replay labels. The main comparisons persist; gating details change. |
| Injection timing (App. K) | post-hoc | Most recoveries at injection index $4$ precede the q-halt plateau; the proxy does not establish an escape mechanism. |
| Expanding-mode control (App. B) | post-hoc, rebuilt | An earlier version returned the opposite verdict; the control families are now pinned by unit tests. |
| Endpoint robustness census | exploratory | Sampling was cut by hand after the problem was seen; it backs no claim here. |

Two departures require disclosure: the regression-rate comparison returned an unanticipated direction, so the lower-regression claim for $z_H$ was withdrawn; the original seed-1 full-clock job did not record its promised reliable-bucket counts. The later refit fills the artifact gap but does not retroactively satisfy the original reporting rule.

## J Compute-matched symmetry-augmentation baseline

Sudoku is invariant under a symmetry group (digit relabeling, band/stack and within-band/stack row/column permutations, transpose): applying any composition to a puzzle yields an equivalent instance whose solution is the transform of the original. For each puzzle in the uniform $N{=}4096$ subset we draw $k{=}8$ seeded random compositions, run the standard $16$-segment forward on each variant, inverse-transform the predicted board, and reselect across the $9$ candidates by max final q-halt (compute-matched to the $z_H$ injection). The transforms round-trip exactly and preserve Sudoku validity (unit-tested).

**What the noise adds on top.** The two arms run on the same uniform subset, so their candidates can be pooled without extra inference: one baseline, 8 symmetry variants, 8 noisy reruns, one max-q-halt argmax over all 17.

| pool | Δ (pts) | gained / lost |
|---|---|---|
| symmetry only ($k$+1) | +34.64 | 1423 / 4 |
| noise only ($k$+1) | +4.76 | 197 / 2 |
| combined (2$k$+1) | +35.16 | 1444 / 4 |
| *marginal of noise* | **+0.51** [+0.29, +0.73] | 21 / **0** |

The marginal is real—the paired interval excludes zero—and it is 21 puzzles. Of the 197 the injection fixes, 176 (89%) are also fixed by some symmetry variant. So against a task-specific baseline that subsumes it, the recurrent-state intervention contributes about a tenth of its standalone +4.8.

On the 962 puzzles outside the nine-orientation oracle union, noise recovers 2.2%, all selected by q-halt. This subset uses ground-truth labels and is a headroom diagnostic, not a deployable selection rule.

**Result.** Exact accuracy 0.416 → 0.762 (+34.6 points, 95% CI [+33.2, +36.1]; 1423 gained, 4 lost, 99.8% retained). Per-cell majority vote across the 9 candidates does *not* help (−1.1 points), so confidence-based selection performs better than this voting rule.

**Validity (not a leak).** Each orientation individually solves ∼41% (baseline 0.416; the eight variants 0.405–0.415), but different orientations solve different puzzles: at least one of the nine is correct for 76.5% of puzzles (the oracle union). The q-halt-chosen accuracy 0.762 sits below this ceiling and recovers 99.6% of it, and *zero* q-halt-chosen predictions are correct outside the union, an internal-consistency check on candidate selection. This check alone does not exclude every possible source of label leakage.

**Overlap.** Symmetry augmentation and noise share 176 recovered puzzles; symmetry uniquely recovers 1247. This demonstrates sensitivity to puzzle orientation, but does not identify an attractor mechanism.

## K INJECTION SITE, TIMING AND RERUN BUDGET

All numbers below (Table 5) use the frozen intervention configuration (noise scale $\varepsilon = 3.0$, injection at zero-based ACT index 4, max-$q$-halt reselection) on the disjoint uniform $N$=4096 subset; only labels enter, as a score. They are a *re-run* of that configuration under a different candidate seed sequence: both runs seed the injection at seed+1 and differ only in the per-candidate stride, so the first of the eight $z_H$ reruns repeats the same noise draw and the other seven are fresh. That is why $z_H$ reads +4.6 (191/2) here against Sec. 8's +4.8 (197/2): the same puzzles under the same procedure, a replication of the perturbation rather than of the sample. The injection index $s_{\text{inject}}$ is zero-based, unlike the segment index $s \in \{1..16\}$ of Sec. 3: $s_{\text{inject}}$=4 injects after five of the sixteen segments have completed, and $s_{\text{inject}}$=0 after one. The two recurrent sites are perturbed at that point; the input embedding is perturbed once before the recurrence starts and the perturbed embedding then drives every step, so the input arm differs from the other two in timing and persistence as well as in site.

Table 5: Reselection by injection site ($k = 8$), using a common absolute noise scale derived from the $z_H$ final update. This corresponds to different relative magnitudes at the three sites. The site-relative comparison below changes the input result from +15.6 to −1.1 points. The small regression counts here do not resolve a difference between recurrent sites; the larger-frame comparison follows.

| site | Δ (pts) | 95% CI | gained | lost |
|---|---|---|---|---|
| $z_H$ (slow state) | +4.6 | [+4.0, +5.3] | 191 | 2 |
| $z_L$ (fast state) | +3.7 | [+3.1, +4.2] | 151 | 1 |
| input embedding | +15.6 | [+14.3, +16.9] | 714 | 75 |

**Regression rates on the full test frame.** Two lost against one, out of $4096$, has no statistical content: at those rates the two sites are indistinguishable below $N \sim 10^5$, and the near-losslessness we claimed for $z_H$ rested on exactly that comparison. Re-running the frozen $k{=}8$ recipe at both recurrent sites on the *full* $422{,}530$-puzzle test frame—nothing was tuned on it, and the prediction frame replays exactly—makes the rates estimable. ($422{,}530$ rather than the $422{,}786$ of Sec. 3: the $256$-puzzle pilot that fixed $\varepsilon$ and the injection segment is held out, so no example that set a hyperparameter is scored here.)

| site | $\Delta$ (pts) | | gained / lost | regression rate, Wilson 95% CI |
|---|---|---|---|---|
| $z_H$ | $+4.36$ | $[+4.30, +4.42]$ | 18,464 / 38 | $0.0090\%$ $[0.0066, 0.0123]$ |
| $z_L$ | $+2.91$ | $[+2.86, +2.96]$ | 12,313 / 15 | $\mathbf{0.0036}\%$ $[0.0022, 0.0059]$ |

The intervals separate, and in the direction opposite to the claim they were run to test. $z_H$ regresses $2.5\times$ as often as $z_L$. So the timescale split does not identify a *safer* site; it identifies a *higher-gain* one, at a measurably higher regression rate. Among recurrent sites there is a trade rather than a free lunch, and we have corrected the main text accordingly. Two things survive: both recurrent sites remain two orders of magnitude safer than the input embedding, which at matched magnitude is net negative; and the $k$-sweep is monotone on the full frame as well ($+1.44$, $+2.28$, $+3.26$, $+4.36$ for $k{=}1, 2, 4, 8$), so extra compute still buys accuracy rather than trading it.

The $k$-sweep at $z_H$ is monotonic: $\Delta = +1.6\,[+1.2, +2.0]$, $+2.7\,[+2.2, +3.2]$, $+3.6\,[+3.1, +4.2]$, $+4.6\,[+4.0, +5.3]$, $+5.8\,[+5.1, +6.5]$ points for $k = 1, 2, 4, 8, 16$, with gained/lost counts $68/1$, $110/1$, $151/2$, $191/2$, $239/2$. The regression count stays at 1–2 throughout, so extra compute buys accuracy without eroding the high observed retention rate. Perturbing $z_L$ is nearly as effective ($+3.7$, $151/1$): a $z_L$ kick propagates into $z_H$ within one H-cycle through the coupling, so it acts as an *indirect* $z_H$ perturbation rather than an independent injection site. We treat the input-injection result cautiously: although its net gain is larger, it perturbs the persistent input drive rather than the recurrent state, testing a different hypothesis (input-space test-time augmentation, the input-perturbation effect independently reported by Ren & Liu (2026)) than the escapability claim; its 75 regressions (against 2 for $z_H$) show it is not the low-regression, mechanism-aligned lever the headline relies on. Per-cell *majority* voting over the same $k{=}8$ reruns is *worse* than baseline ($-0.51$ points, $0.4106$ vs. $0.4158$), the figure Sec. 8 quotes: selection, not agreement, does the work. It is not the $+0.51$ noise marginal of App. J, a different quantity that happens to move the same $21$ puzzles of $4096$.

**Selection rule.** On the same nine symmetry candidates, per-cell majority voting loses $47$ net puzzles ($337$ gained / $384$ lost, $-1.15$ points), whereas max-q-halt gains $34.6$ points ($1423/4$). Thus candidate diversity alone does not explain the low observed regression rate.

**Magnitude-matched sites: the input advantage does not survive.** The comparison above perturbs every site at one common *absolute* scale ($3.0\times$ the median $\|\Delta z_{\text{final}}\|$), which is derived from the $z_H$ update and is therefore not a comparable perturbation at the other two sites. Re-running with each site scaled by its *own* measured radius ($z_H$ by the norm of its final segment-to-segment update, $z_L$ by the norm of its final L-step update, the input by the input-embedding norm; $N{=}4096$, all else frozen) reverses the ordering. The two recurrent radii are measured over different clock intervals, since with $H{=}L{=}2$ one ACT segment contains four L-steps:

| site | $\Delta$ (pts) | gained / lost |
|---|---|---|
| $z_H$ | $+4.6$ | $191/2$ |
| $z_L$ | $+2.9$ | $121/1$ |
| input | $\mathbf{-1.1}$ | $198/\mathbf{243}$ |

The $z_H$ scale is unchanged. Under site-relative scaling both recurrent sites improve accuracy, whereas input injection loses $1.1$ points ($198$ gained / $243$ lost). Site rankings therefore depend on the scale convention. State-update norms and input-embedding norms are different reference quantities; this comparison does not establish a uniquely fair cross-site perturbation metric.

**Between sites, paired on the same puzzles.** Each delta above compares one site to the shared baseline, which orders the sites only indirectly: two intervals that do not overlap are not a test that

one site beats another. Because every rerun's prediction is retained, the sites can be compared directly. Holding the puzzles, the budget ($k$=8) and the site-relative scaling fixed, and scoring the max-q-halt choice at each site against the same labels, McNemar on the paired outcomes gives

| pair | $\Delta$ (pts) | 95% CI | gained / lost |
|---|---|---|---|
| $z_H$ vs. $z_L$ | $+1.68$ | $[+1.20, +2.17]$ | 86/17 |
| $z_H$ vs. input | $+5.71$ | $[+4.60, +6.83]$ | 396/162 |
| $z_L$ vs. input | $+4.03$ | $[+2.95, +5.11]$ | 342/177 |

None of the three intervals covers zero, so at matched radii the ordering $z_H > z_L >$ input is a paired result and not an inference from three separate baselines. The gap between the two recurrent sites is small (1.7 points) beside either one's margin over the input embedding, which is the comparison Fig. 1(a) is drawn to make. This is a within-model ranking at one frozen configuration; it does not carry to TRM, where injecting into either loop gives the same lift (App. V).

**Why the input site fails: the candidates are fine, the ranking is not.** Retaining every rerun's prediction lets us separate the two things a reselection procedure does—generate candidates, and pick one. Write the *oracle union* for the fraction of puzzles some rerun gets right, and ask how much of that reachable headroom max-q-halt actually captures:

| site | $k$ | max-q-halt | oracle union | headroom recovered |
|---|---|---|---|---|
| $z_H$ | 8 | 0.4619 | 0.4624 | **99.0**% |
| $z_H$ | 16 | 0.4736 | 0.4741 | **99.2**% |
| $z_L$ | 8 | 0.4451 | 0.4453 | 99.2% |
| input | 8 | 0.4048 | **0.4839** | **−16.1**% |

Baseline accuracy is 0.4158 ($N = 4096$, site-relative scaling). The final column is the fraction of *oracle headroom* recovered, $(a_{\text{selected}} - a_{\text{base}})/(a_{\text{oracle}} - a_{\text{base}})$, not selected accuracy divided by oracle accuracy. At recurrent sites q-halt recovers about 99% of available improvement. Input injection has the largest oracle union among these three sites, yet selection yields a net loss. This identifies ranking as a limitation at the input site; a distribution shift in the states scored by q-halt is a possible explanation, not a measured causal mechanism.

**Protocol details.** Intervention hyperparameters (rerun count $k = 8$, injection after five ACT segments (zero-based index 4), noise scale $\varepsilon = 3.0 \times \text{median}\|\Delta z_{\text{final}}\|$, and selection by maximum final $q$-halt logit) were tuned on a disjoint 256-example pilot and then *frozen* before the reported evaluation on the uniform $N = 4096$ subset, so no tuning on the reported evaluation subset enters the $+4.76$-point result. The selection rule was chosen by comparison against per-cell majority voting and a $q$-halt gap rule on the pilot; max-$q$-halt was retained based on its pilot performance. Relative ranking across reruns and absolute correctness discrimination are evaluated separately. The stratified per-bucket gains (bucket 1–5 $+56.5$%, 6–20 $+22.9$%, $>20$ $+2.9$%) are much larger than the uniform $+4.76$ points because the stratified sample deliberately oversamples failures; the uniform subset gives the unbiased estimate. Only 2 puzzles were lost against 197 gained, and 99.9% of originally-solved puzzles were retained; regressions are defined relative to the baseline-solved set.

Two mechanisms could explain the Sec. 8 gain: escape from a wrong state whose trajectory has already committed, or ensemble diversity from perturbing a trajectory that has not. To separate them we sweep the injection segment $s_{\text{inject}} \in \{0, 2, 4, 6, 8, 12\}$ with the frozen recipe ($k$=8, $\varepsilon$=3.0×, max-q-halt) on the uniform $N$=4096 subset, holding the injected noise *fixed* across settings so that only the timing varies. For each setting we also record the fraction of gained puzzles whose baseline q-halt trajectory had already plateaued (first reached 95% of its peak rise above segment 0) before the injection point. Read this only as a proxy for a *late, committed* trajectory, not as evidence of stationarity—Sec. 4 measures that directly, and finds most wrong endpoints fail it—so recovery there is the more escape-like of the two mechanisms rather than redirected exploration.

Earlier injection produces larger gains: 9.94 points at $s_{\text{inject}}$=0 versus 1.10 at $s_{\text{inject}}$=12 (Table 6). At the frozen injection index 4, 27% of recovered puzzles had reached the q-halt plateau before injection; at $s_{\text{inject}}$=12, 67% had. Most recovery at injection index 4 therefore occurs before this plateau marker. This is consistent with trajectory diversification, but does not partition the gain

causally into exploration and escape. Earlier injection also allows more continuation, and the same absolute kick can have a different relative scale. The q-halt plateau is not a stationarity certificate.

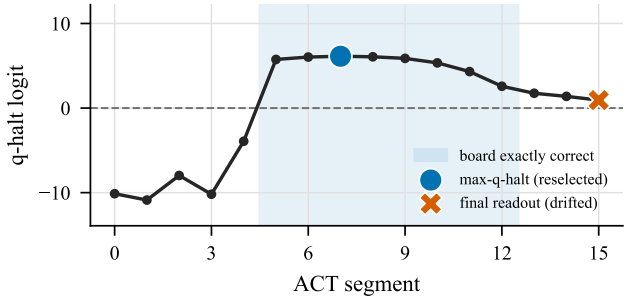


Figure 12: **Why reselection works (one rescued puzzle).** The q-halt logit is deeply negative until the board is exactly correct (shaded), then saturates; the forced final segment has drifted back to wrong, the reselected max-q-halt segment has not.

Table 6: Injection-timing sweep (uniform $N$=4096; noise fixed across rows). $\Delta$ exact accuracy with paired McNemar 95% CI, puzzles gained/lost, and the fraction of gained puzzles whose baseline q-halt had already plateaued before injection (a late-trajectory proxy, not a stationarity test).

| $s_{\text{inject}}$ | $\Delta$ (pts) | 95% CI | gained/lost | plateaued |
|---|---|---|---|---|
| 0 | +9.94 | [+9.01, +10.87] | 412/5 | 0% |
| 2 | +6.47 | [+5.71, +7.23] | 266/1 | 6% |
| 4 | +4.76 | [+4.10, +5.42] | 197/2 | 27% |
| 6 | +4.17 | [+3.56, +4.79] | 172/1 | 38% |
| 8 | +3.05 | [+2.52, +3.59] | 127/2 | 56% |
| 12 | +1.10 | [+0.78, +1.42] | 45/0 | 67% |

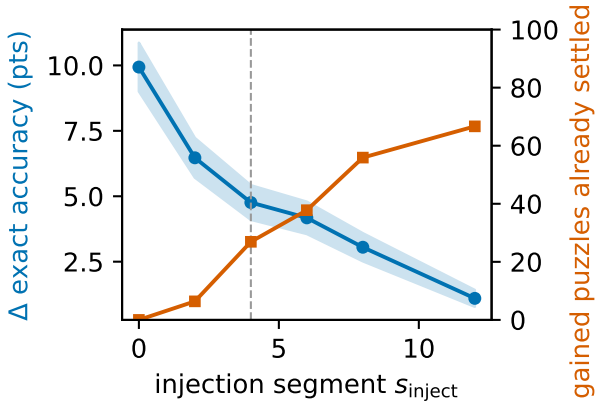


Figure 13: Injection-timing sweep. Blue: $\Delta$ exact accuracy (paired 95% CI band) falls monotonically as the zero-based injection index $s_{\text{inject}}$ (axis label "injection segment") moves later; the dashed line marks the main-text $s_{\text{inject}}$=4. Orange: the fraction of gained puzzles whose trajectory had already plateaued (q-halt plateau—a late-trajectory proxy, not a stationarity test) before injection rises with $s_{\text{inject}}$, so the timing sweep characterises both recovery and its relation to this plateau marker, without identifying an escape mechanism.

## L Compute-matched extended-depth baseline

The $k = 8$ procedure costs 9× inference compute. The depth baseline uses the same budget for a single trajectory of 144 ACT segments. Because the recurrence is a prefix of itself, one 144-segment

pass yields every shorter rung, so the whole ladder is a single sweep ($N$=4096 uniform, seed-0 checkpoint, no perturbation anywhere).

The baselines are matched in total recurrent segment count, not wall-clock latency: extended depth executes 144 sequential segments, whereas perturb-and-reselect executes nine 16-segment trajectories whose independence permits concurrent evaluation. With sufficient accelerator capacity, concurrency can reduce response time at the cost of greater simultaneous activation memory; our experiments do not establish a measured parallel speedup. Extending the depth also requires no extrapolation of a learned clock encoding. The exogenous clock denotes the prescribed update schedule, and the segment index is not supplied to the recurrent modules. The extended-depth baseline repeats the same weight-shared updates with the unchanged $H = 2, L = 2$ schedule, carrying both latent states forward; positional encodings remain tied to puzzle positions. No segment-index clipping, modulo operation, or state reset is applied at the training horizon. Nevertheless, execution beyond the 16 training segments can encounter unfamiliar latent states. We therefore treat the 144-segment run as a horizon-extrapolation baseline: its reported accuracy measures the utility of continued recurrence at matched computation, without assuming unchanged representation quality or equivalent deployment latency.

The injection arm in this comparison is the frozen recipe ($+4.8$), not the sweep maximum of $+9.94$ at $s_{\text{inject}}$=0 (App. K), which is matched on budget too. We compare against the frozen arm because its $(\varepsilon, s_{\text{inject}})$ was fixed on a disjoint pilot before this evaluation, whereas the sweep maximum is selected post-hoc over six values on the evaluation subset itself and carries the corresponding optimism. Read as a ceiling rather than a protocol, well-timed injection exceeds extended depth at the same budget.

| segments | $\Delta$ (pts) | 95% CI | gained / lost |
|---|---|---|---|
| *read out at the final segment* | | | |
| 144 | $+5.6$ | $[+4.9, +6.4]$ | $245/14$ |
| *max-q-halt segment of the same single pass* | | | |
| 144 | $\mathbf{+6.0}$ | $[+5.3, +6.7]$ | $\mathbf{248/2}$ |
| *oracle: any segment of the pass correct* | | | |
| 144 | $+6.1$ | $[+5.4, +6.8]$ | $249/0$ |

This is a genuine head-to-head: the ladder draws the *same* uniform subset as the injection arm (valid examples only, tuning pilot excluded, same seed), and the baselines agree to one puzzle—$0.41602$ against $0.41577$.

At the matched $9\times$ budget, final-segment depth gains $5.6$ points and depth with segment selection gains $6.0$, versus $4.8$ for the frozen noise recipe. Segment selection recovers $248/249$ oracle-recoverable puzzles and reduces regressions from 14 to 2. These are observed comparisons on this sample, not a proof of oracle-optimal selection. The 245 wrong-to-right changes under final-segment readout show that some terminal errors can be corrected by continued recurrence; they do not exclude later convergence to other attractors.

## M UNPERTURBED CONTINUATION CONTROL

The $\varepsilon = 0$ control continues each terminal state without a kick. It distinguishes ordinary continuation from perturbation-induced displacement. The initial full-trajectory sample contains 32 solved and 32 mild-wrong endpoints, with 12 noise seeds and scale $\kappa = 2.391$; the deterministic control is run once per endpoint.

| $\varepsilon$ | solved $R_{\text{state}}$ | wrong $R_{\text{state}}$ | median $d/d_0$ (solved) | median $d/d_0$ (wrong) |
|---|---|---|---|---|
| 0 (no perturbation) | 0.8125 | 0.1250 | 1.000 | 1.000 |
| $1.0\times$ | 0.8125 | 0.1250 | 1.004 | 1.000 |
| $19.95\times$ | 0.8099 | 0.1250 | 1.008 | 1.000 |

Here $d_0$ is the displacement under unperturbed continuation. At the largest radius the median solved displacement is $1.008d_0$; the wrong-class ratio remains $1.000$. The mild-wrong answer-persistence rate is $0.375$ without perturbation, consistent with the perturbed sweep. Thus continuation dominates

the tested perturbation effect. This pilot uses the same severity bucket as the main text, but fewer endpoints.

**Re-measured at $16\times$ the endpoints.** Because the pilot showed little sensitivity to radius, we allocated more computation to endpoints—$\varepsilon{=}0$ plus one perturbed radius, at $512$ endpoints per class—and report percentile bootstraps clustered on endpoints, since the seeds of one endpoint share its geometry:

| class | $R_{\text{ans}}$ | $R_{\text{state}}$ | $n$ |
|---|---|---|---|
| solved | $0.953\,[0.934, 0.971]$ | $0.856\,[0.824, 0.885]$ | 512 |
| wrong, 1–5 | $0.418\,[0.347, 0.494]$ | $0.129\,[0.082, 0.182]$ | 170 |
| wrong, 6–20 | $0.088\,[0.047, 0.135]$ | $0.047\,[0.018, 0.082]$ | 170 |
| wrong, >20 | $0.041\,[0.017, 0.076]$ | $0.035\,[0.012, 0.064]$ | 172 |
| wrong, pooled | 0.182 | 0.070 | 512 |

The pilot mild rate lies inside the larger sample's interval. Solved and mild-wrong intervals are disjoint, and the mild upper bound is $0.494 < \frac{1}{2}$. Mild failures are the most persistent wrong bucket. This ordering does not distinguish boundary sensitivity from continued state motion. In the separate replay audit (App. H), $27.8\%$ of dump-labelled mild endpoints re-decode as solved. Error count does not measure distance to a decode boundary, and becoming fully solved on replay is a different event from preserving the entire decoded answer under continuation. The observed severity ordering therefore does not exclude boundary sensitivity as a contributor to answer non-persistence. The pooled $0.182$ is a mixture over the sampled severities, not a test-population-weighted wrong-answer rate. The severity ordering changes under replay labels (App. H).

These results support answer non-persistence at the tested horizon. They do not measure basin depth, prove noise has no effect at other scales, or identify the mechanism of mid-trajectory reselection.

**It replicates on a second seed and a second architecture.** Unperturbed continuation returns the perturbed rates again on the seed-1 checkpoint ($0.81/0.09$ against a perturbed median $0.81/0.10$; median $d/d_0 \le 1.05$) and on TRM ($0.23/0.03$ against $0.22/0.04$; $d/d_0 \le 1.09$). So the perturbation failing to matter is a property of these recurrences, not of one checkpoint. (TRM's absolute rates here differ from the $0.32/0.02$ quoted in App. V, which was measured on a different stratified sample; the $\varepsilon{=}0$ vs. $\varepsilon{>}0$ comparison is within-run and unaffected.)

The perturbation sweep is therefore a robustness check on the continuation measurement. Both class separation and its interpretation should be assessed within each checkpoint and sampling protocol.

## N Continuation to 128 times the trained budget

The unperturbed control removes the perturbation as the cause of the motion. It does not remove the *horizon*. Our stationarity test continues for one more budget (16 segments), so it establishes that a wrong terminal state is not stationary *at that horizon*, and a state can lie inside a basin without having arrived. A reader is entitled to ask whether these states simply converge later, to a wrong answer. We therefore continued them, with no perturbation, to $512$ segments: $32\times$ the trained budget, reading the state out at $16/32/64/128/256/512$. Solved states were run identically as a control. This and the $2048$-segment run below are horizon extrapolations on the same terms as App. L: no segment index enters the recurrent modules, so nothing is clipped or wrapped, but the latent states reached late in these runs are further outside anything training visited than at $144$ segments. Drift measured there may reflect that distance rather than the dynamics the trained regime would show.

| $T$ | 16 | 32 | 64 | 128 | 256 | 512 |
|---|---|---|---|---|---|---|
| *answer unchanged since the previous read-out* | | | | | | |
| solved | 0.92 | 0.97 | 0.97 | 0.97 | 0.97 | **0.97** |
| wrong | 0.16 | 0.33 | 0.34 | 0.42 | 0.44 | **0.45** |
| *answer unchanged since the terminal state* | | | | | | |
| solved | 0.92 | 0.92 | 0.92 | 0.92 | 0.92 | 0.92 |
| wrong | 0.16 | 0.16 | 0.19 | 0.19 | 0.17 | 0.16 |
| *exact-correct* | | | | | | |
| wrong | 0.23 | 0.23 | 0.25 | 0.28 | 0.30 | 0.30 |

The pilot uses $n = 64$ per class. Wrong-answer persistence remains below solved persistence, but successive-readout rates cannot be compared directly because their intervals differ. We therefore extend continuation to 2048 segments with equal 128-segment windows ($n = 64$ per class; wrong endpoints pooled over all three severity strata). Selected checkpoints are shown below; each rate compares to the readout 128 segments earlier, including checkpoints not printed in the table.

| $T$ | 128 | 256 | 512 | 1024 | 1536 | 2048 | mean 256–2048 |
|---|---|---|---|---|---|---|---|
| wrong | 0.19 | 0.44 | 0.44 | 0.44 | 0.45 | 0.41 | **0.43** |
| solved | 0.92 | 0.97 | 0.97 | 0.97 | 0.97 | 0.97 | 0.97 |

Across the fifteen windows after the first, wrong-answer persistence ranges from 0.39 to 0.45 (mean 0.43, fitted slope $+0.0002$ per window), versus 0.97 for solved endpoints. Wrong-class exact accuracy stabilises around 0.28–0.30. There is no detectable increasing persistence over this measured horizon.

A pre-specified control expected the solved-state residual to decay toward zero. The recorded quantity does not: it remains about 0.99 of its first-readout value through 512 segments. That quantity is not the one-step residual the control named. It is the displacement between successive readouts, $\|z_H(T) - z_H(T_{\text{prev}})\|$, normalised by the first readout's class median, over windows that grow through $16/16/32/64/128/256$ segments. A displacement measured over windows of changing length does not fix a per-segment rate, so we read no convergence verdict from it. Complex eigenvalues alone also do not establish a limit cycle. We therefore do not infer a rotating attractor from this observation.

Finite continuation cannot exclude slower convergence, periodic dynamics, or an attractor reached beyond 2048 segments. The supported conclusion is persistent answer changes over the observed windows, not the absence of asymptotic attractors.

## O NONLINEAR CORRECTNESS READOUTS

Sec. 4 reports that a *linear* probe on the final $z_H$ barely outperforms the model's own halting head, and we drew no design conclusion from that, because testing one probe family licenses none. Fitting the missing families settles it. Features are a *trajectory summary* the $z_H$ probe never sees—the per-segment halt and continue logits and the four sublayer update norms at every recorded tick (800 features)—on the same 1024-state stratified sample, stratified 5-fold cross-validated, scored out-of-fold, with bootstrap CIs over states:

| readout | AUROC (all) | | AUROC (mild only) | |
|---|---|---|---|---|
| q-halt (the model's own) | 0.934 | [0.916, 0.951] | 0.873 | [0.835, 0.909] |
| linear, trajectory | 0.956 | [0.943, 0.968] | 0.919 | [0.891, 0.943] |
| MLP (64, 32) | 0.966 | [0.956, 0.976] | 0.942 | [0.923, 0.959] |
| gradient-boosted trees | **0.969** | [0.958, 0.979] | **0.944** | [0.921, 0.962] |

Both feature choice and model class contribute. A linear trajectory readout improves mild-failure AUROC from the terminal-state probe's 0.887 to 0.919; boosted trees on those same trajectory features reach 0.944. The latter exceeds q-halt's 0.873, with non-overlapping reported intervals. This is evidence of recoverable correctness information beyond the tested terminal-state linear probe, not an attribution solely to nonlinearity. The detector uses signals already produced by the model, although recording them and fitting the readout incur additional cost. Its across-puzzle discrimination is distinct from q-halt's performance ranking reruns of one puzzle.

Decodability also emerges gradually over the iteration, rising from AUROC $0.61$ at iteration 0 to $0.91$ mid-trajectory and $0.94$ at the end, mirroring the contraction toward the low-residual endpoint.

*Scope, and an artifact gap we should state.* $n$=1024 from the stratified sample, one checkpoint, one task; no hyperparameter search was performed, so these nonlinear models should be read as untuned reference families rather than optimized predictors. The three fitted rows were re-derived after the fact and now have stored metrics; the original fit was run outside our analysis pipeline and its outputs were never kept, so feature construction and folds were reconstructed from this description rather than recovered. Read them as an independent re-derivation. The ordering and the q-halt comparison are unchanged by it; the values moved by at most $0.011$. The $800$ trajectory features still come from a residual-stream pass we do not persist (Reproducibility Statement), so reproducing them means re-running from the checkpoint. The q-halt row is quoted from the relabelling audit of App. H, which stores it; the same logit captured inside the re-derivation scores $0.935/0.857$, and the audit's $0.873$ sits inside that run's mild interval $[0.813, 0.897]$.

## P THREE ROBUSTNESS CHECKS: KRYLOV DIMENSION, TRAINING MATURITY, SECOND SEED

**Is the spectral separation an artifact of the Krylov dimension?** Every radius we compute in this paper is a leading-Ritz estimate from an $m$-step Arnoldi factorization with $m$=40, apart from the two sensitivity runs in this paragraph; the third-party GRAM pilot of App. T reports $\hat{\rho}_{80}$. Re-running the endpoint sweep at $m$=20 and $m$=80 leaves the class separation intact and moves the wrong-class maximum by less than $10^{-7}$:

| $m$ | solved $\bar{\rho}$ | wrong $\bar{\rho}$ | wrong max | $n$/class |
|---|---|---|---|---|
| 20 | 0.419 | 0.754 | 1.166 | 128 |
| 40 (paper) | 0.442 | 0.749 | 1.166 | 256 |
| 80 | 0.427 | 0.757 | 1.166 | 128 |

The $\rho$=1.17 endpoint is therefore not a subspace-truncation artifact: doubling and halving the Krylov dimension moves it in the eighth decimal (1.1661161 at $m$=40 and $m$=80, 1.1661162 at $m$=20). *Caveat:* the $m$=20 and $m$=80 runs used 128 endpoints per class against the main run's 256, so the *tail counts* across rows are not a matched comparison and we do not read the solved-side counts ($0/128$, $0/128$ against $2/256$) as evidence about the solved outliers.

**Does the timescale split decay with training maturity?** A reasonable worry is that the fast/slow dissociation is a late-training artifact of a fully-trained network. It is not; it is present at all four training steps we refit (held-out hi-energy $R^2$). The four step rows share one labelled manifest built from the final seed-0 checkpoint, so each is fitted on the fixed cohort of puzzles the final checkpoint solves rather than on a checkpoint-specific solved stratum. The seed-1 row uses seed 1's own labels:

| step | fast $z_L$ | slow $z_H$ | gap |
|---|---|---|---|
| 15,624 | 0.73 | 0.47 | +0.26 |
| 26,040 | 0.87 | 0.37 | +0.50 |
| 36,456 | 0.78 | 0.33 | +0.45 |
| 52,080 (paper) | 0.72 | 0.37 | +0.35 |
| seed 1, 52,080 | 0.61 | 0.31 | +0.30 |

The gap is large and positive throughout, and non-monotone rather than decaying, so the split is a property of the trained recurrence and not of the particular stopping point we analyse. The last row is a different *seed* rather than a different step: refitting the whole clock on seed 1's own sample returns $+0.30$, so the split survives a change of initialisation as well as of stopping point. That row carries the caveat of its own $n$, discussed next.

**Second seed.** A seed-1 retrain (final exact accuracy $48.67\%$) reproduces the intervention, more strongly than seed 0: $z_H$ gives $+6.6$ points (274 gained, 2 lost), $z_L$ $+6.0$ ($252/6$), input $+16.6$ ($697/19$). These numbers are scored against seed 1's *own* predictions and are sound. We no longer

read the 2-vs-6 split as evidence that $z_H$ is the safer site: at $N{=}4096$ those counts are not separable, and on the full frame the ordering runs the other way (App. K).

The *stratified* geometry replicates too, and more sharply than on seed 0. The two $R$ rows are the $n{=}32$-per-class full-trajectory set of App. M, which is why they read $0.97/0.38$ rather than the $0.95/0.42$ of Sec. 4's $512/170$ frame; the comparison is seed-to-seed within a row.

| | seed 0 | seed 1 |
|---|---|---|
| endpoint $\bar{\rho}$ (solved / wrong) | 0.44 / 0.75 | 0.44 / **0.85** |
| $\hat{\rho}_{40}{>}1$ (solved / wrong) | $2/256$ / $7/256$ | $3/128$ / $\mathbf{27}/\mathbf{128}$ |
| gate-passing (solved / wrong) | 0.95 / 0.69 | 0.95 / **0.49** |
| $R_{\text{state}}$ (solved / wrong) | 0.81 / 0.12 | 0.81 / **0.09** |
| $R_{\text{ans}}$ (solved / wrong) | 0.97 / 0.38 | 0.88 / **0.16** |

Every direction the paper claims survives the seed change, and the $\hat{\rho}_{40}{>}1$ tail—which we report two-sided throughout—is far more asymmetric here (21% of wrong against 2% of solved) than on seed 0. The $\varepsilon{=}0$ result replicates as well: unperturbed continuation gives $0.81/0.09$ against a perturbed median of $0.81/0.10$, with median $d/d_0$ at most 1.05.

**Checkpoint-specific strata.** Seed-1 analyses use labels from seed 1's own predictions. Reusing seed-0 strata mixed solved and wrong endpoints and produced misleadingly similar answer-persistence rates ($0.74/0.72$). Rebuilding the sample restored the contrasts above. Each replication therefore requires its own labelled manifest.

## Q N-QUEENS 12-BY-12: LOW-ACCURACY TRAINING AND A NULL INTERVENTION

Because every headline number in this paper is Sudoku, we pre-specified a third task chosen to stress a property Sudoku lacks: N-Queens $12{\times}12$ has 14,200 complete boards in all, and each given-constrained puzzle admits a subset of them, so a correct model need not reproduce the labelled one. The plan, fixed in advance, set the board size, the scoring (a board is *valid* if it places exactly 12 non-attacking queens and keeps every given queen; *canonical* if it equals the labelled solution), and the read: if both accuracies came out low, the verdict was underfit and the run should go to the compute cap rather than be reported as a finding about dynamics.

That is what happened. Trained to the cap on a single RTX 6000 Ada (15h25m), the model reaches 0.22% canonical exact and 1.78% *any* valid board (1.56% valid-but-non-canonical). A stratified draw for the failure analysis found only **2** canonically-solved puzzles in the pool, against 14 valid-non-canonical, 17 near-misses and 481 far-misses, so there is no solved class to compare a wrong class against, and none of the three analyses in this paper can be run. The reselection arm is correspondingly null: over 900 multi-solution puzzles, $k{=}8$ gives $\Delta_{\text{any}}{=}{+}0.22$ points (95% CI $[-0.21, +0.66]$) and solution-set coverage moves $0.50\% \to 0.73\%$ against a deterministic ceiling of 28.6%.

The null bounds the task coverage: this checkpoint provides too few canonical successes for the planned class comparisons. Differences in task, scoring and data generation prevent attributing the result to augmentation multiplicity alone.

**A data-matched control, and what it does and does not explain.** To separate the data regime from the task we rebuilt Sudoku at N-Queens' budget (5,000 puzzles with 5 augmentations each, 30,000 rows in 5,000 groups) and trained the byte-identical released recipe. Test exact accuracy, scored on the full 422,786-puzzle frame:

| epoch | exact | cell acc. | test loss | $q$-halt acc. |
|---|---|---|---|---|
| 2000 | **4.26%** | 0.617 | 1.46 | 0.996 |
| 4000 | 3.45% | 0.607 | 1.78 | 0.986 |
| 6000 | 3.61% | 0.606 | 1.91 | 0.961 |

Training exact accuracy reaches 0.99–1.00, while test accuracy remains 3.45–4.26%. This indicates a generalisation gap under the smaller Sudoku data regime. The run ended at approximately 39% of

the schedule, so later improvement cannot be excluded. The matched-size Sudoku result shows that low accuracy is not inevitable at this example count, but cross-task differences in solution multiplicity and scoring prevent isolating a task-specific cause for the N-Queens null.

## R MAZE REPLICATION ACROSS TRAINING CHECKPOINTS

We re-run the headline analyses on a second weight-tied task, Maze-30×30-Hard (sequence length 900, vocabulary 6), under the *identical* released configuration ($H$=2, $L$=2, ACT max 16). Our single-GPU cluster cannot reach the paper's multi-GPU Maze-Hard accuracy, so we analyse two points on one $\mathrm{gbs}$=32 trajectory: epoch 4000 (uninterrupted; $1.5\%$ exact) and a warm-restart continuation to epoch 7000 (re-warmed LR; $10.7\%$ exact). Both are under-trained, so this is a reduced-scale check of whether the *dynamics* transfer, not a performance replication. Protocols are unchanged; the timescale test leans on the reliable unsolved stratum (512 mazes, $R^2_{\mathrm{corr}}{\approx}1$), the solved strata being thin (15 mazes at epoch 4000). Stored metrics now cover the spectra, persistence, full-clock fits and intervention results (Tables 8, 7, 9).

**Endpoint spectra do not decide here, and say something else instead.** We ran the endpoint Jacobians under the usual protocol on *all* 107 solved mazes in the test set and 128 wrong ones ($m$=40). The ordering is **undecided**: $\hat{\rho}$ averages 1.003 solved against 1.023 wrong, $+0.020$ with SE 0.024 (95% CI $[-0.027, +0.066]$; medians 0.960 vs. 0.966), and it is not monotone in wrongness—the mildest bucket averages 0.998, *below* solved. The Sudoku gap is 0.307, fifteen times larger on comparable $n$. We report this as underpowered rather than as a refutation, the branch specified in advance for a solved class this small, and mark the cell in Fig. 15. The solved side is a *census*: at $10.7\%$ exact there are only 107 solved mazes, so this power cannot be bought with a larger draw, only with a better checkpoint.

What the same numbers do establish is not about the ordering. Both classes sit at $\hat{\rho} \approx 1.0$, so here a *solved* maze is not the stable rotating contraction a solved Sudoku is (0.44); it is marginal. With the answer-level rates above—solved mazes reproduce their own answer 0.60 of the time against Sudoku's 0.97—two independent measurements agree that this network's correct answers are not settled states. That is consistent with settling being something a recurrence acquires with competence (App. Q), and is why the low *absolute* rates in Table 8 are the expected reading rather than a failure of the criterion. Which of the two causes—different task, or under-training—produces the marginality, one such checkpoint cannot say.

**Attenuation is the fast loop moving, not the split dissolving.** The split reproduces at epoch 4000—a $+0.37$ gap against Sudoku's $+0.41$, both fits reliable—and the later checkpoint has a gap of $+0.04$. The $\Delta$ row of Table 7 says how: the slow loop is *unchanged*, and the whole collapse is the fast loop becoming less linearisable. The model therefore becomes *less* captured by the tested linear families with more training, the opposite of the training-phase artifact that the bare gap collapse would otherwise suggest. What we cannot separate is "more training" from the LR re-warm, which returned to peak and could itself perturb the dynamics.

**The intervention transfers; its accounting does not.** $z_H$-noise reselection lifts exact accuracy $+3.5$ points (Table 9), essentially Sudoku's $k$=4 figure ($+3.6$). The regressions are what does not transfer, and the raw counts understate it because the frames differ in size: $42/7$ on $N$=1000 against $151/2$ on $N$=4096 is a loss *rate* of $0.70\%$ against $0.049\%$, $14\times$ higher. The 0.099 baseline is the instrumented loop's score, $\sim$0.8 points below the training-eval $10.7\%$—the loop-vs-loop difference verified to `bfloat16` tolerance in the reproducibility statement.

**Net.** Split, intervention and the solved-vs-wrong basin ordering all appear on a second task. A *fully-trained* Maze is what would settle the three things this checkpoint leaves open: whether the split persists under unperturbed training, whether the endpoint ordering exists, and whether the marginal spectra are the task or the under-training. App. S reports training without a warm restart and its full-clock refit. The split persists, but the runs also differ in training length and accuracy, so the cause of the magnitude change remains unresolved.

Table 7: Maze full-clock *held-out* hi-E $R^2$ (Algorithm 1, as Table 1). **The $\Delta$ row is the result:** between the two points $z_H$ does not move and the whole gap collapse is $z_L$ becoming *less* linearisable. Sudoku: unsolved 0.80/0.39 (+0.41), solved 0.72/0.37 (+0.35). † epoch-4000 solved is 15 mazes ($z_H$ $R^2_{\text{corr}}$=0.29); read the *unsolved* block.

| stratum | training point | $z_L$ | $z_H$ | gap |
|---|---|---|---|---|
| unsolved | epoch 4000 (1.5%) | 0.94 | 0.57 | +0.37 |
| | epoch 7000 (10.7%) | 0.61 | 0.57 | +0.04 |
| | $\Delta$ | **−0.33** | **0.00** | **−0.33** |
| solved | epoch 4000† | 0.90 | 0.21† | +0.69 |
| | epoch 7000 | 0.59 | 0.46 | +0.13 |

Table 8: Maze reproduction at both levels (Sec. 4; epoch 7000; 96+96 states, 8 seeds, isotropic $z_H$ noise at 5 radii × median $\|\Delta z_{\text{final}}\|$; 768 continuations per class per radius). Both levels order the classes and both are flat in $\varepsilon$—the scale-invariance the main text reports for Sudoku, and the only reason five radii are shown. The last column is Sudoku-HRM on its $n$=32-per-class set, printed beside rather than in prose for what it exposes: **every Maze *solved* $R_{\text{state}}$ cell sits below Sudoku's *wrong*** 0.12, so no absolute threshold separates the classes across settings, while the within-setting ordering holds in all of them.

| | class | 0.1 | 0.32 | 1.0 | 3.2 | 10 | *Sudoku* |
|---|---|---|---|---|---|---|---|
| $R_{\text{state}}$ | solved | 0.095 | 0.095 | 0.096 | 0.098 | 0.079 | *0.81* |
| | wrong-FP | 0.027 | 0.027 | 0.026 | 0.025 | 0.022 | ***0.12*** |
| $R_{\text{ans}}$ | solved | 0.599 | 0.583 | 0.600 | 0.600 | 0.590 | *0.97* |
| | wrong | 0.301 | 0.301 | 0.276 | 0.260 | 0.275 | *0.38* |

## S MAZE TRAINING WITHOUT A WARM RESTART

To test whether the warm restart explained the reported 10.7% Maze accuracy, we ran the same configuration without restarting optimisation. Resume sidecars preserve optimizer moments, step count, data-loader position and provenance; resuming without a sidecar is rejected. Two 23-hour single-GPU jobs reached epoch 13,500 (421,875 steps), versus the original 7000 epochs. The second job resumed from step 406,250.

The recipe uses `lr_min_ratio=1.0`: after 2000 warmup steps, the logged learning rate stays at $10^{-4}$. A warm restart therefore repeats warmup and resets Adam moments, rather than restarting a decaying learning-rate schedule.

Across 25 evaluations from epoch 1500 to 13,500, exact accuracy ranges from 0.3% to 27.0%, with median 13.0% and no clear upward trend. The original 10.7% is within this range and recurs at epoch 11,000. Cell accuracy varies less (0.949–0.978); whole-maze correctness magnifies these differences across 900 cells. This run does not support warm restart as the sole explanation for low accuracy, but it is not a controlled estimate of its causal effect.

The pre-specified 40% accuracy target was not reached. Maze therefore remains a reduced-scale replication.

**The full-clock refit this run was missing.** Refitting the final no-restart checkpoint (step 421,875, 23.0% exact on the 1000-maze test split) gives held-out hi-energy $R^2$ of 0.856 for $z_L$ against 0.465 for $z_H$ on solved states, a gap of +0.391, and 0.857 against 0.500 on unsolved (+0.357). The published checkpoint reads +0.129 and +0.038. The split therefore also appears in the no-restart run, with the same sign and a larger observed magnitude. This comparison does not identify the causal effect of the restart on the gap.

Three qualifications travel with that. The two runs differ in three ways at once, restart, length and accuracy, so this is not a controlled estimate of the restart's effect on the gap any more than the accuracy comparison above was. The 23.0% is one draw from a band this run swings across without

Table 9: Maze $z_H$-noise reselection (epoch 7000; $k$=4, $s_{\text{inject}}$=4, $\varepsilon$=3.0×, max-q-halt; $N$=1000, the full test set). Baseline is the paired instrumented re-run. Sudoku at $k$=4: $+3.6$ $[+3.1, +4.2]$ (App. K); the $k$=8 headline is $+4.76$.

| baseline | chosen | Δ (pts) | 95% CI | gained/lost |
|---|---|---|---|---|
| 0.099 | 0.134 | +3.5 | [+2.15, +4.85] | 42/7 |

trend, so it is not evidence of a better-trained Maze. And the gaps do not order with accuracy across the three Maze checkpoints we have:

| checkpoint | exact | solved $z_L$ / $z_H$ | gap |
|---|---|---|---|
| step 125,000 | 1.5% | 0.901 / 0.212 | +0.689 |
| step 218,750 (published) | 10.7% | 0.590 / 0.462 | +0.129 |
| step 421,875 (no restart) | 23.0% | 0.856 / 0.465 | +0.391 |

Steps 125,000 and 218,750 are one lineage either side of the warm restart and step 421,875 is a separate run, so these three points span two optimisation histories rather than one, and the non-monotonicity is not a trend. What survives is the sign, positive in all three, on the 11/5 and 7/2 reliable high-energy buckets the clock affords here. The attenuation Sec. 6 reports is a property of the published checkpoint, not of the task.

## T GRAM ENDPOINT PILOT AND GRAM-GUIDED TRM

Maze (App. R) changes the task and holds the architecture fixed; this appendix and App. V change the *architecture*. Here it is GRAM, the stochastic latent recurrence of Baek et al. (2026) (not the unrelated architectures sharing that acronym). This leg is deliberately small and is reported for one reason: it produced a methodological warning that does not depend on its sample size, and that we then had to apply to TRM.

Read the two halves separately. The protocol comparison is a *population* measurement over the full held-out splits ($n$=773 and $n$=578); the spectral half is a balanced $n$=2-per-cell pilot that establishes wiring, not effect sizes.

**The sampler is load-bearing (Table 10).** Collapsing the stochastic transition to its conditional mean costs 49.8 points on N-Queens ($0.964 \to 0.466$) and 71.5 on edge-colouring. Whatever the latent recurrence is doing, sampling is part of it.

Table 10: Solve rate of the *same* checkpoint under three noise protocols, prescanned over the whole held-out split (not the $n$=2 spectral strata, so these rates are population-level). Sampled inference reproduces the independently recorded single-draw scores (0.952 and 0.670), a harness check; collapsing the sampler to its conditional mean is catastrophic.

| noise protocol | N-Queens ($n$=773) | edge-col. ($n$=578) |
|---|---|---|
| conditional mean ($\xi$=0) | 0.466 | 0.005 |
| quenched $T$-periodic | 0.696 | 0.291 |
| sampled inference | **0.964** | **0.720** |

**No ordering claim, in either direction.** A stochastic map has no single endpoint Jacobian, so the endpoint protocol has to be read through a forcing choice (Table 11). Three of the four cells interleave the validity strata outright. The fourth orders them the *wrong* way and rests on a valid stratum drawn from 3 eligible items in 578, with 2 batch-vs-single replay mismatches among 129 candidates checked. At $n$=2 per cell one cannot detect an ordering that exists, so we claim none. What the sample does support is the weaker and here sufficient statement that a contracting endpoint is not by itself evidence of correctness, which Sec. 5 reaches for HRM from the opposite side, a wrong terminal state there carrying a perfectly contracting local linearisation.

Table 11: Endpoint leading-Ritz estimates (median of $n$=2 per cell) for the bare conditional $f_H$ map, the conditional $f_L$ map, and the joint supervision-step map, with the joint map's fixed-point residual. The last column states the $f_H$ verdict for the valid/invalid pair it heads, read off the two raw per-item radii rather than the medians: "none" means the strata's radii interleave, so the pair carries no ordering. Only one of the four pairs orders, and it orders the *wrong* way (v>i: valid $\{1.09, 1.34\}$ above invalid $\{0.86, 1.07\}$) in the one block where nothing is near a root. † marks cells whose residual makes the radius an endpoint linearisation only, not a stability claim; the $12.85$ entry is the median of $\{0.95, 24.75\}$ and the $24.75$ state has both the run's largest residual ($0.61$) and its largest $m$-to-$m$ spread ($2.9\times10^{-2}$).

| | | $\hat{\rho}_{80}$ | | | joint | $f_H$ |
|---|---|---|---|---|---|---|
| protocol | stratum | $f_H$ | $f_L$ | joint | residual | order |
| *N-Queens* | | | | | | |
| mean | valid | 0.79 | 0.69 | 0.94 | $2\times10^{-2}$ | none |
| mean | invalid | 0.80 | 1.46 | $12.85^{\dagger}$ | $3\times10^{-1}$ | |
| quenched | valid | 0.75 | 0.47 | **0.23** | $3\times10^{-5}$ | none |
| quenched | invalid | 0.76 | 0.78 | **0.38** | $5\times10^{-5}$ | |
| *edge-colouring* | | | | | | |
| mean | valid | $1.21^{\dagger}$ | 0.88 | $1.87^{\dagger}$ | $3\times10^{-1}$ | v>i$^{\dagger}$ |
| mean | invalid | $0.97^{\dagger}$ | 1.15 | $1.01^{\dagger}$ | $3\times10^{-1}$ | |
| quenched | valid | 0.85 | 0.61 | **0.75** | $2\times10^{-3}$ | none |
| quenched | invalid | 0.80 | 1.37 | $1.05^{\dagger}$ | $6\times10^{-2}$ | |

**Residuals and forcing protocol.** Under quenched forcing on N-Queens, the 16-step stroboscopic map has relative residuals 3.2–8.7 $\times$ $10^{-5}$ on all four tested states and leading-Ritz estimates in $[0.19, 0.57]$, for both valid and invalid answers. Under the conditional-mean protocol, residuals reach $0.61$ and one radius estimate reaches $24.75$. These are different deterministic maps. Large-residual endpoints cannot support a fixed-point stability interpretation; small residuals and finite-Krylov spectra are supporting diagnostics, not certificates. The TRM analysis likewise reports its spectra both before and after residual-based gating (App. V).

**Scope of the pilot.** 2 items per (protocol $\times$ validity) cell, hence 8 endpoint records per task; effect-size estimation requires a larger, purpose-designed sample. Nothing in the main text rests on these numbers, and the edge-colouring results appear in Fig. 15 not at all and only here. As in the main text $\hat{\rho}_{80}$ is a finite-Krylov estimate over a 69,632- or 81,920-dimensional state, not a certified radius. Unlike the HRM and TRM legs this one runs against a third-party checkpoint through a GRAM-side script that is not ours: we record the checkpoint, dataset and analysis-code hashes with the metrics, but that leg cannot be re-run from our own materials alone. That is why it stays a pilot, and why the figure's row is no longer built from it.

**GRAM-guided TRM.** We train a reproducible GRAM-guided TRM on N-Queens-$10 \times 10$ with `gram_guidance=true`, $\beta = 0.005$, guidance on $z_H$, $H = 3$, $L = 6$ and 16 ACT segments. It reaches $38.5\%$ canonical exact accuracy and $50.4\%$ any-valid accuracy. At evaluation guidance is the deterministic update $z_H \leftarrow z_H + \mu_p(z_H)$. The original persistence sweep omitted $\varepsilon = 0$. A separate control on the same checkpoint gives answer persistence $0.98/0.84$, close to the perturbed rates below, supporting a continuation-based interpretation.

Answer persistence is $0.98/0.84$ for solved/invalid boards, and state persistence is $0.92/0.20$ (768 continuations per class per radius). Reselection gains $5.4$ points (95% CI $[4.4, 6.4]$, $112/2$, $N = 2048$). The raw endpoint-radius ordering reverses ($1.02$ solved versus $0.75$ wrong; $t = -11.3$, 256 endpoints per class), as does the full-clock split ($R^2 = 0.83$ fast versus $0.96$ slow). The additive guidance update is a possible contributor to the high slow-loop predictability; its causal contribution has not been isolated.

The terminal-update gate passes $94.9\%$ of solved and $96.5\%$ of wrong endpoints. Together with the high wrong-answer persistence, this limits generalisations of the HRM failure pattern. It also

demonstrates that high terminal persistence can coexist with gains from an earlier intervention: the two experiments measure different behaviours.

**Forward-pass parity.** Earlier analysis replicas omitted the guidance step at the end of each segment. This produced invalid but plausible metrics, including an endpoint ordering of the opposite sign. Those artifacts are retained as superseded and are not used here. All five analysis paths now call the same recurrence function. The parity check covers the intervention rollout and the endpoint rollout, precedes the analysis chain, and gives cell agreement $1.000000$. It does not cover the instrumented full-clock driver, which carries the guidance shift forward but records each $z_H$ snapshot at the output of `L_level`. The guidance update is therefore folded into the following tick rather than given a tick of its own, and all fifteen high-energy $z_H$ buckets behind the $0.96$ above carry that folded tick on one side of their regression.

## U Relation to prior accounts of failure

The accounts reviewed in Sec. 2 motivate a distinction between within-budget trajectory geometry and persistence beyond the terminal readout. Sghaier et al. (2026) discuss bounded non-convergence; Corbett et al. (2026) discuss continued exploration and provide local tube-stability and guide-alignment diagnostics. These accounts need not describe mutually exclusive behaviours.

**Source scope.** The full text of Efstathiou & Balwani (2026) is behind an access challenge we could not clear, so everything we attribute to it comes from its published abstract, which states all three of the claims at issue: that "failed runs plateau at stable high-loss attractors rather than continuing exploration", that trajectories "descend into local minima determined by initialization", and that the intervention is "adding noise to answer initialization and scaling guess attempts". We make no claim to have verified the experiments behind them, and we do not describe those experiments. The distinction our measurement turns on survives either way: changing an initial state can select a different basin even when attractors are stable, so a successful initial-state perturbation does not test terminal-state stability.

**Different stability quantities.** The tube-stability result of Corbett et al. (2026) assumes contraction along a neighbourhood of the deterministic trajectory and estimates local secant ratios for its diagnostics. Our Arnoldi calculation estimates leading eigenvalues at selected endpoints. A spectral-radius estimate is not a uniform operator-norm bound, and a small terminal residual does not certify a fixed point. Our measurements therefore neither verify that theorem's assumptions nor establish their failure on the checkpoints used there. Instead, Sec. 4 directly measures whether a terminal decoded answer survives a specified continuation, with an unperturbed control. Its finite horizon limits conclusions about asymptotic attraction.

**Candidate generation and selection.** Both prior studies distinguish available candidates from the selector's ability to recover them. On Maze, Sghaier et al. (2026) report $11.83$ points of pass-at-$K$ improvement but only $1.37$ points with halting-head selection; Corbett et al. (2026) report guided accuracy $85.3\%$, below the $86.6\%$ deterministic baseline despite a $90.9\%$ oracle. Our contribution is complementary paired accounting and site comparisons.

For HRM/Sudoku ($N = 4096$, $k = 8$), we retain each candidate's final q-halt logit and compare within-puzzle spread between baseline errors for which some rerun is correct and errors for which none is correct:

| site | rescuable wrong (median q-halt SD) | stuck wrong (median SD) | ratio |
|---|---|---|---|
| $z_H$ | 6.22 ($n$=191) | 0.42 ($n$=2202) | 14.8× |
| $z_L$ | 6.05 ($n$=121) | 0.32 ($n$=2272) | 18.9× |
| input | 5.65 ($n$=279) | 1.48 ($n$=2114) | 3.8× |

Recurrent-site logit spread is larger for recoverable errors. Input injection produces more spread overall but a smaller contrast between the groups and worse selected accuracy (App. K). These associations support examining guide alignment alongside candidate diversity; spread alone does not

establish correct ranking. The corresponding rescuable-versus-unrecoverable comparison has not been measured on Maze or TRM.

## V TRM REPLICATION WITH SHARED MODULES

The pilot in App. T changes the architecture but keeps two *separate* modules. This appendix removes the degree of freedom the main text leans on hardest—the two modules themselves—at full protocol strength. TRM (Jolicoeur-Martineau, 2025) is the strongest form of Sec. 9's question—*one shared network* $f$ drives both states on the same nested clock structure as HRM, $z_L \leftarrow f(z_L, z_H + e_x)$ run $L{=}6$ times then $z_H \leftarrow f(z_H, z_L)$ once, for $H{=}3$ high-level cycles per segment over 16 segments. We train it to $87.31\%$ exact on Sudoku-Extreme (matching the paper's $\sim 87.4\%$). Its own published ablation is independent training-side evidence for the reading here: replacing the 1-step gradient with backpropagation through the whole final high-level cycle, its $z_L$ updates together with the $z_H$ update that follows them, lifts accuracy $56.5 \rightarrow 87.4$. The earlier high-level cycles still run under `no_grad` and the carry is detached between segments, so the comparison shows that non-terminal updates carry learned computation inside one cycle rather than locating it across the whole trajectory. We re-run all three headline analyses verbatim on the EMA checkpoint, with the instrumented loop bit-exact to the model's own forward. Figure 14 previews the headline: the found/not-found spectral split is the mirror image of HRM's.

**On unsolved states the timescale split inverts (Table 12).** Under the same held-out full-clock refit as Sec. 6, the *fast* $z_L$ loop is the *less linearisable* stream (unsolved $R^2{=}0.45$, $n{=}48$ reliable high-energy buckets, split-half $R^2_{\text{corr}}{=}0.97$) and the *slow* $z_H$ loop the more linear ($0.62$, $n{=}2$, $0.99$)—the mirror image of HRM's unsolved fast $0.80 \gg$ slow $0.39$. The robust anchor is the well-powered fast-$z_L$ estimate ($0.45$, far below HRM's unsolved $0.80$); the slow-loop number rests on the two reliable high-energy buckets the slow stream admits—a structural readout limit stable across independent samples, not a tuned cut. Sharing the module does not preserve the fast-more-linearisable/slow-less-linearisable dissociation on unsolved states; it *inverts* it there, and ties on solved.

Table 12: TRM held-out high-energy per-tick linear $R^2$ (full-clock refit) at two sample sizes, with HRM for reference. In TRM the fast $z_L$ loop is the *less linearisable* stream on the unsolved stratum—the inversion—and that survives a $4\times$ larger sample. $n$ is the count of reliable high-energy buckets surviving the $0.3$ reliability-ceiling cut; the retained count need not grow with sample size.

| | $N{=}1024$ | | $N{=}4096$ | |
|---|---|---|---|---|
| | fast $z_L$ | slow $z_H$ | fast $z_L$ | slow $z_H$ |
| TRM, solved | 0.43 (92) | 0.35 (13) | 0.48 (87) | 0.48 (3) |
| TRM, unsolved | 0.45 (48) | 0.62 (2) | 0.45 (48) | 0.60 (2) |
| HRM, solved | **0.72** | 0.37 | — | — |
| HRM, unsolved | 0.80 | 0.39 | — | — |

**Reliable-tick coverage.** Increasing the sample from 1024 to 4096 leaves the unsolved slow-loop estimate at two reliable high-energy ticks and changes its $R^2$ from $0.62$ to $0.60$. The solved slow-loop count changes from 13 to 3, and its initial fast–slow gap disappears ($0.48/0.48$ at $N = 4096$). The reported inversion is therefore restricted to the unsolved stratum.

Tick count is bounded by the clock (47 slow versus 287 fast ticks), but the number passing the reliability floor can depend on sample size and thresholds. The larger run does not establish that no further sample could improve coverage. HRM's default slow-loop aggregate also uses only 1–3 ticks; App. F reports how relaxing the thresholds increases coverage. Conclusions concern the ordering under the stated estimator, with limited slow-tick coverage.

**Persistence and raw spectra.** TRM answer persistence is $0.96$ solved versus $0.32$ wrong, and state persistence is $0.32/0.02$ (Table 13). The wrong class pools all three severity buckets (96 endpoints per class); the HRM pilot uses only mild failures (32 per class). Thus the protocols share radii and criteria, but their absolute rates are not a severity-matched comparison. A mild-only TRM rate cannot be inferred from HRM's severity pattern.

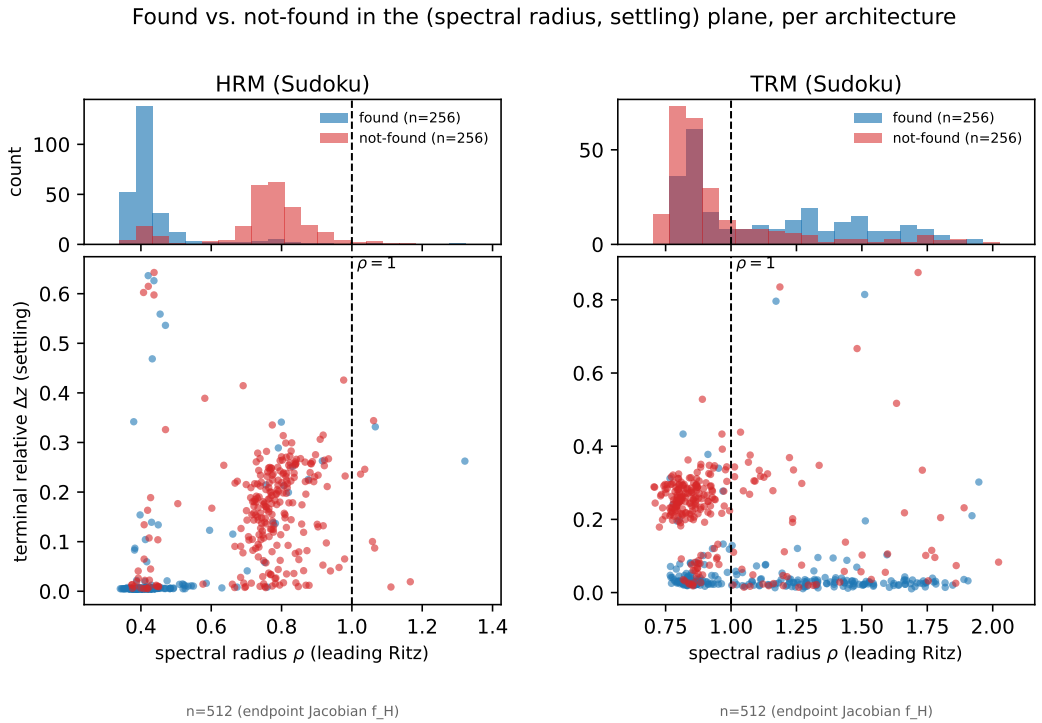


Figure 14: **The inversion, per instance.** Every evaluated puzzle placed by its endpoint Jacobian spectral radius $\rho$ (leading Ritz, $x$) and terminal relative update (settling, $y$), coloured by whether the model found the solution; top strips are the $\rho$ histograms. *HRM* (left): found answers contract to a tight $\rho \approx 0.4$, low-residual cluster and failures spread toward $\rho$=1. *TRM* (right): the ordering *inverts*—found answers sit at $\rho$>1 (marginally expanding) yet still clear the terminal-update gate (low residual), while failures fall to *lower* $\rho$; the metastable high-residual band (red) survives in both. That drop is carried by the high-residual band: gated to states that pass the terminal-update gate, the two TRM strata coincide (see text). Tables 12–13 made per-instance. ($n$=512 per architecture.)

Both original sweeps omit $\varepsilon = 0$ and retain only radius aggregates, so endpoint-clustered intervals cannot be recovered from those artifacts. Separate unperturbed controls are reported in App. M. The raw TRM leading-Ritz means are $1.15$ solved and $0.96$ wrong (wrong maximum $2.02$), with correlation $-0.42$ between radius and gate failure. These local estimates do not establish attractor stability.

**The residual gate dissolves the inversion.** Only $24\%$ of the $256$ wrong TRM endpoints pass the terminal-update gate. Applying Eq. 7 with TRM's own solved calibration ($q_{95} = 0.148$) gives mean radii $1.149$ for wrong endpoints ($n = 62$) and $1.151$ for solved endpoints ($n = 243$). The reported unrounded difference is $0.003$ ($95\%$ bootstrap CI $[-0.09, 0.09]$; Mann–Whitney $p = 0.57$). The excluded $194$ wrong endpoints have mean radius $0.90$ and account for the raw reversal. HRM retains a gated difference ($0.43$ solved, $n = 243$, versus $0.73$ wrong, $n = 176$; $p < 10^{-40}$). Thus no spectral ordering is detected in gate-passing TRM endpoints. Because the gate is calibrated to solved residuals, passing it does not certify that an endpoint is a root.

**Reselection at both TRM sites (Table 14).** On $N = 2048$ puzzles, injecting $z_L$ gains $8.25$ points ($95\%$ CI $[7.1, 9.4]$, $169/0$); injecting $z_H$ gains $8.40$ ($172/0$). Their baselines differ slightly ($0.852$ and $0.849$), and we do not have a paired between-site test establishing equivalence. The observed gains provide no clear evidence that the less-linearisable stream is the preferred site. Perturbation and halting-head selection are established in Sghaier et al. (2026), which reports $87.28\% \rightarrow 98.75\%$ at a larger budget; these are different protocols and checkpoints.

Table 13: TRM endpoint geometry under Sec. 4's stability test, with HRM anchors. Every cell is a class *mean* ($\bar{\rho}$, gate-passing) or the median over the 13-radius sweep ($R_{\text{ans}}$, $R_{\text{state}}$); no column mixes a mean with a max. The solved-vs-wrong ordering agrees between the two models in every column but $\bar{\rho}$, whose sign flips (and vanishes under the gate); $R_{\text{ans}}$ admits the better-separated threshold for these two settings: $\frac{1}{2}$ leaves all four cells at least $0.12$ from the cut, while a state-level cut of $0.22$ separates the same four cells with a margin of $0.10$. Neither cut travels beyond these two settings (Fig. 15). The $\bar{\rho}$ column is *ungated* and averages gate-passing and gate-failing endpoints together; after gating the TRM rows coincide ($1.151$ vs $1.149$) and only the gate-passing fraction still separates them. Severity coverage of the two wrong rows differs (see text).

| | $\bar{\rho}$ | gate-passing | $R_{\text{ans}}$ | $R_{\text{state}}$ |
|---|---|---|---|---|
| TRM, solved | 1.15 | 0.95 | 0.96 | 0.32 |
| TRM, wrong | 0.96 | 0.24 | 0.32 | 0.02 |
| HRM, solved | 0.44 | 0.95 | 0.97 | 0.81 |
| HRM, wrong | 0.75 | 0.69 | 0.38 | 0.12 |

Table 14: Oracle-free noise-injection + halting-logit reselection, TRM (inject the fast $z_L$ loop) vs HRM (inject the slow $z_H$ loop). Each injects into the loop its own full-clock refit finds least linearisable. In TRM the two loops are indistinguishable as sites ($+8.25$ vs. $+8.40$), so that choice is not what carries the gain there.

| | site | exact | $\Delta$ (95% CI) | gained/lost |
|---|---|---|---|---|
| TRM | $z_L$ | .852→.934 | $+.083\,[+.071, +.094]$ | 169/0 |
| TRM | $z_H$ | .849→.933 | $+.084\,[+.072, +.096]$ | 172/0 |
| HRM | $z_H$ | — | $+.048\,[+.041, +.054]$ | 197/2 |

**Additional coverage qualifications.** N-Queens-$10 \times 10$ has answer-persistence rates $0.96/0.56$ for solved/wrong endpoints. Valid but non-canonical boards give $0.93$, close to the solved rate; they should not be interpreted as constraint violations. Input injection gives the largest observed gain on this task ($8.8$ points), so the preferred HRM injection site does not transfer. The N-Queens and GRAM-guided sweeps omit $\varepsilon = 0$; separate unperturbed controls on the same checkpoints return answer persistence $0.97/0.59$ and $0.98/0.84$. Each control is one deterministic continuation per endpoint ($64$ per class), not the $768$ continuations behind the perturbed cells.

The Maze full-clock and intervention cells and the seed-1 full-clock cell are stored metrics, not values quoted from manuscript tables: the seed-1 refit records $11$ reliable fast buckets against $1$ slow bucket, and the Maze epoch-$7000$ refit $18$ against $3$. The third-party GRAM endpoint pilot and the GRAM-guided TRM replication are distinct experiments (App. T); their results must not be used interchangeably.

**Cross-architecture scope.** Solved–wrong persistence ordering and positive reselection gains appear in all six settings, but state-persistence thresholds use setting-specific scales ($\kappa = 1.4$–$47$, across $81$–$900$ positions). The answer-level $\frac{1}{2}$ cut also fails on both N-Queens settings, despite their newly measured unperturbed controls. Endpoint and full-clock patterns transfer less consistently. Both TRM variants differ from HRM in several respects, so module sharing is not isolated as a cause; GRAM-guided TRM also lacks HRM's terminal-gate separation ($94.9\%$ solved / $96.5\%$ wrong). Finally, TRM's two injection sites yield similar gains despite different linearity estimates. The transferable observation is the persistence ordering, not a universal spectral, residual or optimal-injection-site rule.

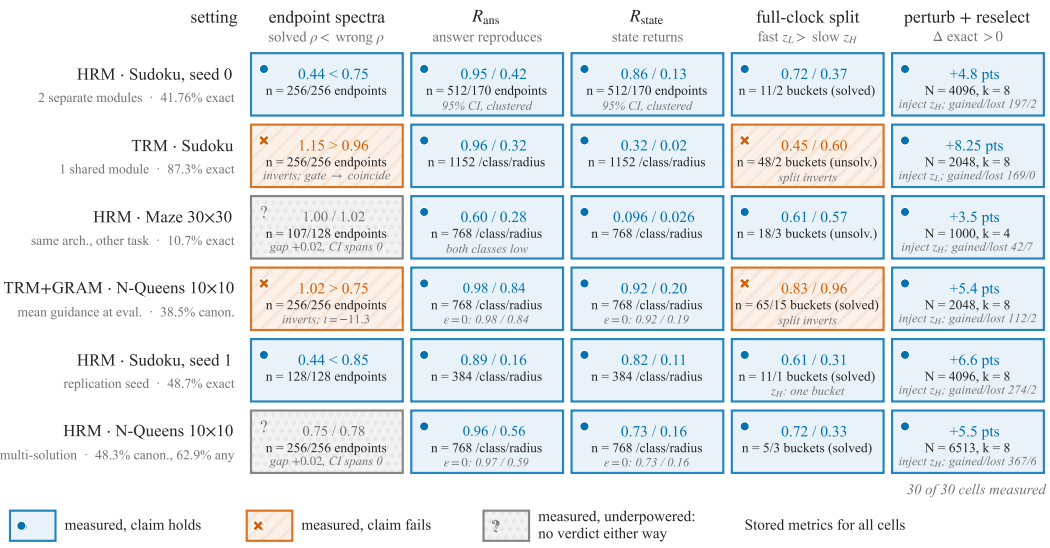


Figure 15: **Coverage across six evaluated settings.** Columns report endpoint spectral ordering, the full-clock split, state persistence, answer persistence and reselection gain. Discs indicate the specified comparison holds, crosses that it fails, and question marks that the measurement is inconclusive. Each cell reports its sample or tick count; all cells now have stored metrics. Persistence columns denote solved–wrong ordering, not a universal $\frac{1}{2}$ threshold. That threshold fails for N-Queens and GRAM-guided TRM. The TRM spectral inversion is ungated and disappears after gating; its full-clock inversion occurs only in the unsolved stratum. N-Queens-$12 \times 12$ and the third-party GRAM endpoint pilot are reported separately in Apps. Q and T.